

REPORT DOCUMENTATION PAGE			Form Approved OMB NO. 0704-0188	
Public Reporting burden for this collection of information is estimated to average 1 hour per response, including the time for reviewing instructions, searching existing data sources, gathering and maintaining the data needed, and completing and reviewing the collection of information. Send comment regarding this burden estimates or any other aspect of this collection of information, including suggestions for reducing this burden, to Washington Headquarters Services, Directorate for information Operations and Reports, 1215 Jefferson Davis Highway, Suite 1204, Arlington, VA 22202-4302, and to the Office of Management and Budget, Paperwork Reduction Project (0704-0188,) Washington, DC 20503.				
1. AGENCY USE ONLY (Leave Blank)		2. REPORT DATE 26 June 2001		3. REPORT TYPE AND DATES COVERED Final Report for 31 March 2000-30 March 2001
4. TITLE AND SUBTITLE High-Temperature Gel Permeation Chromatography System for Optical Polymers Research			5. FUNDING NUMBERS DAAD19-00-1-0074	
6. AUTHOR(S) Shaw H. Chen				
7. PERFORMING ORGANIZATION NAME(S) AND ADDRESS(ES) Department of Chemical Engineering, University of Rochester Room 1210, COI, 240 East River Road Rochester, New York 14623-1212			8. PERFORMING ORGANIZATION REPORT NUMBER DURIP-99-Final Report	
9. SPONSORING / MONITORING AGENCY NAME(S) AND ADDRESS(ES)  U. S. Army Research Office P.O. Box 12211 Research Triangle Park, NC 27709-2211			10. SPONSORING / MONITORING AGENCY REPORT NUMBER DOD/ARMY/ARO  40862.1-CH-RIP	
11. SUPPLEMENTARY NOTES The views, opinions and/or findings contained in this report are those of the author(s) and should not be construed as an official Department of the Army position, policy or decision, unless so designated by other documentation.				
12 a. DISTRIBUTION / AVAILABILITY STATEMENT  Approved for public release; distribution unlimited.			12 b. DISTRIBUTION CODE	
13. ABSTRACT (Maximum 200 words)  A high-temperature gel permeation chromatograph has been acquired for the measurement of absolute molecular weight distribution to support a MURI Program on <i>Tunable Optical Polymer Systems</i> . Conjugated polymers have been actively pursued over the past two decades for electronic, optical, photonic, and optoelectronic applications. In the last few years, liquid crystalline conjugated polymers have begun to attract attention because of their ability to self-organize. One can now imagine taking advantage of the new optical properties originating in ordered conjugated systems. <i>Nonmesogenic conjugated</i> polymers are known to effect electrochromism and voltage-tunable light emission, and <i>nonconjugated mesogenic</i> liquid crystals (chiral-nematics in particular) are known to effect tunable selective reflection. As a major challenge, <i>chiral-nematic conjugated</i> polymers are being designed and synthesized to accomplish all three modes of tunability across the visible and infrared region for defense and civilian applications. In addition, we are developing novel conjugated oligomers configured in a three-dimensional space to effect control of nanoscale morphology critical to optoelectronic properties, for which a manuscript is attached to illustrate our molecular design concept.				
14. SUBJECT TERMS conjugated polymers and oligomers tunable optical properties light absorption, emission, and reflection liquid crystalline conjugated polymers			15. NUMBER OF PAGES 43	
			16. PRICE CODE	
17. SECURITY CLASSIFICATION OR REPORT UNCLASSIFIED	18. SECURITY CLASSIFICATION ON THIS PAGE UNCLASSIFIED	19. SECURITY CLASSIFICATION OF ABSTRACT UNCLASSIFIED	20. LIMITATION OF ABSTRACT  UL	

20010731 125

MEMORANDUM OF TRANSMITTAL

U.S. Army Research Office  
ATTN: AMSRL-RO-RI. Mrs. Sylvia Hall  
P.O. Box 12211  
Research Triangle Park, NC 27709-2211

☐ Reprint (Orig + 2 copies)

☐ Technical Report (Orig + 2 copies)

☐ Manuscript (1 copy)

☒ Final Progress Report (Orig + 2 copies)

☐ Related Materials, Abstracts, Theses (1 copy)

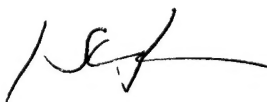
CONTRACT/GRANT NUMBER: DAAD10-00-1-0074

REPORT TITLE: *High-Temperature Gel Permeation Chromatography System for Optical Polymers Research*

is forwarded for your information.

SUBMITTED FOR PUBLICATION TO (applicable only if report is manuscript):

Sincerely,



Shaw H. Chen

Professor Shaw H. Chen  
Department of Chemical Engineering  
Room 1210 COI, University of Rochester  
240 East River Road  
Rochester, New York 14623-1212

**FULLY SPIRO-CONFIGURED TERFLUORENES AS  
NOVEL AMORPHOUS MATERIALS EMITTING BLUE LIGHT**

<sup>¶</sup>Yanhou Geng, <sup>¶</sup>Dimitris Katsis, <sup>¶</sup>Sean W. Culligan,  
<sup>¶</sup>Jane J. Ou, <sup>¶</sup><sup>‡</sup>, \*Shaw H. Chen, and <sup>§</sup>Lewis J. Rothberg  
Departments of <sup>¶</sup>Chemical Engineering and <sup>§</sup>Chemistry  
<sup>‡</sup>Laboratory for Laser Energetics

Center for Optoelectronics and Imaging, University of Rochester  
240 East River Road, Rochester, New York 14623-1212

\* Author to whom correspondence should be addressed.

Submitted to *J. Am. Chem. Soc.*

June 2001

## ABSTRACT

A series of fully spiro-configured terfluorenes were synthesized and characterized to be amorphous materials showing a  $T_g$  of 296 °C with dendritic aromatic pendants, the highest value ever reported for organic molecular systems. X-ray single crystal analysis of key structural moieties indicated nearly perpendicular orientations at all spiro-links. The spectroscopic comparison of solid film and dilute solution suggested absence of aggregates in the ground state and no increase in torsion angle with an increasing volume of the aromatic pendant. All these conformational characteristics are consistent with molecular mechanics simulation. Thermal annealing in argon caused a decrease in fluorescence yield with phenyl pendants but an increase with dendritic pendants. These can be understood in terms of local morphological reorganization of molecules to enhance or inhibit interactions between the backbone chromophores.

## INTRODUCTION

Conjugated polymers represent one of the most extensively investigated classes of advanced materials in recent years. Reasons for the extraordinary intensity of interest include: the diverse structures and properties afforded by molecular design and synthesis; the ease of processing and low costs compared to inorganic materials; and the technological potential for electronics, optics, photonics, and optoelectronics [1]. In particular, feasibility has been demonstrated for light-emitting diodes [2], organic lasers [3], thin film transistors [4], photoconductors [5], and nonlinear optical devices [6]. Recent studies have uncovered the importance of interchain interactions and nanoscale morphology in conjugated polymer films to photophysical properties [7, 8]. Conjugated oligomers have a number of advantages over polymers both for scientific understanding and device work: solubility, purity, and ease of characterization. In addition, conjugated oligomers have well-defined structures with few defects to permit structure-property relationships to be systematically investigated [9]. However, oligomers are limited by (i) a tendency to crystallization, yielding a polycrystalline film unsuitable for device application because of light scattering and/or poor charge carrier mobility, and (ii) a low glass transition temperature,  $T_g$ , in comparison to polymers. Recently, several distinct classes of glass-forming conjugated oligomers with an elevated  $T_g$  have been successfully synthesized: star-burst molecules (or dendrimers) [10] with a  $T_g$  up to 134 °C, spiro-linked oligo(*p*-phenylene)s [11] and oligo(triphenylamine)s [12] with a  $T_g$  up to 236 °C and 133 °C, respectively, and tetrahedrally-configured oligo(*p*-phenylene-vinylene)s [13] with a  $T_g$  up to 230 °C.

Our goal in the present study was to combine the promise of poly(fluorene)s as efficient and stable blue light-emitters [14-18] with recent successes in the development of functional molecular glass for optoelectronics [10-13, 19-21]. Additionally, we incorporated pendant groups to suppress interchromophoric interactions that cause reduced emissive efficiency [22] and color instability [23]. Dendritic pendants to poly(*p*-phenylenevinylene) [24] and poly(fluorene) [25] have been found to be effective in suppressing these unfavorable interactions. In what follows we report on novel terfluorenes in which all the monomer units are spiro-configured to achieve an elevated  $T_g$  while minimizing interchromophoric interactions that occur through  $\pi$ -stacking.

## RESULTS AND DISCUSSION

Fully spiro-configured terfluorenes **1a**, **1b**, and **1c** as shown in Chart 1 were synthesized according to Reaction Scheme 1. Each molecule comprises two spiro-linked terfluorene segments. Terminal fluorene units are further spiro-linked to aromatic pendants with an increasing volume from a phenyl group in **1a**, a *p*-terphenyl group in **1b**, to an aromatic dendron in **1c**. Intermediates **6a**, **6b**, and **6c** were synthesized from 2-bromofluorene and **4a**, **4b**, and **4c** in 50, 65, and 58%, respectively. Intermediate **7b** was prepared as a boronic ester, instead of a boronic acid as **7a** and **7c**, to overcome the solubility problem. The target compounds, **1a**, **1b**, and **1c** were synthesized with the Suzuki coupling reaction [26] at a 71, 39, and 61% yield, respectively. While **1a** and **1c** were found to be readily soluble in chloroform, methylene chloride and tetrahydrofuran, **1b** showed limited solubility presumably because of the linear and rigid *p*-terphenyl group. Molecular structures were elucidated with elemental analysis,  $^1\text{H}$ - and

$^{13}\text{C}$ -NMR spectroscopy, as illustrated respectively in Figures 1 and 2 for **1c**. The three  $^{13}\text{C}$ -signals at  $\delta$  45.82, 56.74, and 66.43 ppm are attributable to three types of nonaromatic carbon atoms associated with the spiro-centers.

Based on previously reported X-ray single crystal analysis of 9,9'-spirobifluorene [27], the two spiro-linked fluorene units without any substituent groups are oriented at  $87.7^\circ$ . X-ray analysis of single crystals of **6a** (0.20 mm $\times$ 0.20 mm $\times$ 0.40 mm), as shown in Figure 3, further corroborates the molecular structure; it also reveals a  $90.3^\circ$  and  $144.6^\circ$  orientation between the two planes meeting at C-11 and those intersecting at C-14 and C-21, respectively. These analytical data combine to depict **1a**, **1b**, and **1c** as molecular systems meeting our objective of preventing  $\pi$ -stacking of the fluorene chromophores. The basic idea is visualized in Figure 4A, where spiro-links are shown as crosses with *p*-terphenyl groups and aromatic dendrons depicted as long bars and circular plates, respectively. Single crystals of **1a**, **1b**, or **1c** were not successfully prepared for X-ray analysis. Instead, molecular mechanics simulation was performed on the three terfluorenes using the Amber software package together with the Alchemy force-field parameters. The energy-minimized structures are presented in Figure 4B. All three compounds were found to possess approximately the same conformational characteristics. The planes intersecting at all five spiro-centers were found to be oriented at  $90^\circ$  in all three terfluorenes. Based on carbon atoms numerically identified in Figure 3, the plane defined by C(11, 14, 21) makes a  $146\pm 3^\circ$  angle with the one by C(14, 15, 20, 21), which is roughly coplanar with the phenyl ring comprising C(15–20). A nearly constant torsion angle between neighboring fluorene units,  $42\pm 3^\circ$ , also emerged from simulation, a value consistent with  $40^\circ$  reported for hexaoctyl terfluorene [28]. The terfluorene segments in **1a**, **1b**, and **1c** are

responsible for a UV-Vis absorption peak at  $358\pm 2$  nm, in dilution solution and in neat film (see Supporting Information), indicating a torsion angle independent of the aromatic pendant's volume. In a nutshell, key conformational features furnished with X-ray crystal analysis and UV-Vis absorption spectroscopy are in good agreement with molecular mechanics simulation.

Thermal analysis was carried out with a combination of differential scanning calorimetry and hot-stage polarizing optical microscopy. Pristine samples of **1a** and **1c** were found to be amorphous in the process of heating to 370 °C, whereas that of **1b** showed a crystalline melting peak at 465 °C. These samples were subsequently cooled at  $-200$  °C/min to  $-30$  °C before recording the second heating scans at 20 °C/min. The thermograms presented in Figure 5 indicate that **1a** and **1c** undergo glass transitions at 225 and 296 °C, respectively, whereas **1b** undergoes a glass transition at 275 °C followed by recrystallization at 328 °C and crystalline melting at 452 °C. The  $T_g$  of 296 °C exhibited by **1c** is the highest ever observed of organic molecular systems. Heating **1a** and **1c** to 370 °C as part of the thermal analysis did not result in thermal decomposition, as evidenced by  $T_g$ s determined from the third heating scans remaining to within  $\pm 1$  °C of those from the second heating scans. However, heating **1b** up to 480 °C, necessitated by its high crystalline melting point, apparently caused thermal decomposition, as evidenced by a depression in the melting peak by 6 °C on the third heating scan compared to the second heating scan.

In comparison to previously reported conjugated oligomers with a single spiro-link [11, 12], all the fluorene units in oligomers **1a**, **1b**, and **1c** are spiro-configured to minimize  $\pi$ -stacking. Films of **1a** and **1c** were prepared by spin-coating from a 1 wt% solution in chloroform with



subsequent vacuum drying at room temperature overnight, giving rise to a thickness on the order of 100 nm. The UV-Vis absorption spectra of solid films of **1a** and **1c** showed no shift from a peak at 358 nm observed in chloroform at  $10^{-5}$  M, indicating absence of ground-state interactions to form aggregates in neat film. With photoexcitation at 350 nm, films of **1a** and **1c** produced qualitatively identical emission spectra but with a 10 to 14 nm red-shift from dilute solution (two peaks at 393 nm and 414 nm) probably due to energy migration to the more planar chromophores in the excited state. Since benzylic hydrogens are known to be prone to photooxidation, precautions were taken to minimize degradation as a result of UV-exposure in air by limiting the fluorescence measurement time to 1 min. Enclosing films in a cell through which a constant flow of argon was maintained produced identical fluorescence spectra. The limited solubility of **1b** prevented film preparation by spin-coating for investigation of light absorption and emission.

The UV-Vis absorption and photoluminescence spectra of solid films are presented in Figure 6, in which the amorphous character is shown with electron diffractometry to persist upon thermal annealing under argon at 100 °C for 96 h (see insets). Furthermore, it is demonstrated that thermal annealing did not result in an appreciable change in the absorption spectra. However, significant modifications of fluorescence intensity were observed: a 25% decrease in emission intensity in the case of **1a**, but a 50% increase in the case of **1c**. In either case, no emission peak beyond 500 nm appeared, as encountered with thermal annealing or photooxidation of varied poly(fluorene)s [15, 23, 29-31]. As a typical example of emission spectral instability, poly(fluorene) functionalized with n-hexyl groups showed a growing extent of excimer emission, with thermal annealing, as a broad peak at 530 nm at the expense of blue emission [32]. A reduced emission intensity of **1a** upon prolonged heating could have arisen from enhanced

interchromophoric interactions, resulting in a long tail in the emission spectrum (see Figure 6A) and quenching through the formation of nonemissive excimers. A plausible explanation for an increased emission intensity as a result of thermally annealing **1c** is that energetically favored dendritic stacking suppresses interchromophoric quenching between fluorene units. The above interpretation is motivated by two observations: (i) that the dendritic pendants in **1c** are more inclined to stacking than the isolated phenyl pendants in **1a**, and (ii) that stacking of the aromatic dendrons is expected to prevent fluorene units from  $\pi$ -stacking because of the nearly perpendicular orientation between the two planes meeting at C-11 and those intersecting at C-14 and C-21 (see Figure 2).

To compare total emission affected by prolonged heating, fluorescence quantum yield ( $\eta$ ) was measured relative to 9,10-diphenylanthracene doped in a poly(methylmethacrylate) film at  $10^{-2}$  M. For the measurement of  $\eta$ , the refractive index dispersion,  $n(\lambda)$ , is needed as input to Eq.(2) in the Experimental Section. The results determined with variable angle spectroscopic ellipsometry are included as insets in Figure 6. An  $\eta$  value of 0.83 was found for **1a** in a 0.5  $\mu\text{m}$  thick poly(methylmethacrylate) film at a  $10^{-2}$  M doping level, for which the refractive index was also measured with the same technique. Upon prolonged heating under argon, a neat film of **1a** (76 nm thick) exhibited an  $\eta$  decreasing from 0.28 to 0.24, whereas a neat film of **1c** (124 nm thick) an  $\eta$  increasing from 0.16 to 0.24. It is evident that concentration quenching is responsible for the diminished  $\eta$  in neat films compared to a lightly doped poly(methylmethacrylate) film.

## SUMMARY

An effective approach to high glass-transition terfluorenes has been successfully implemented in which all the fluorene units are spiro-configured to prevent interchromophoric interaction without disrupting  $\pi$ -conjugation. Novel material systems were synthesized with molecular structures elucidated by elemental analysis,  $^1\text{H}$ - and  $^{13}\text{C}$ -NMR spectroscopy. A  $T_g$  of 296 °C was achieved with dendritic pendants to spiro-linked fluorene trimers, which was found to be amorphous upon prolonged heating under polarizing optical microscopy and electron diffractometry. Single crystal analysis of key structural moieties and molecular mechanics calculations of target molecules revealed nearly perpendicular orientations at all spiro-links. All three terfluorenes showed a UV-Vis absorption peak at  $358\pm 2$  nm in dilute solution and in neat film, indicating absence of ground-state aggregation in solid state and no increase in torsion angle with an increasing volume of the aromatic pendant. The conformational characteristics derived from X-ray crystal analysis and UV-Vis absorption are consistent with molecular mechanics simulation. In comparison to the fluorescence spectra in dilute solution, pristine films showed a 10 to 14 nm red-shift presumably due to energy migration to the more planar fluorene chromophores in the excited state. Heating solid films under argon at 100 °C for 96 h resulted in similar fluorescence spectra to pristine films without excimer emission as a broad peak at 530 nm characteristic of varied poly(fluorene) films. However, the emission intensity was found to decrease with phenyl pendants, which was attributable to the formation of nonemissive excimers. In contrast, the emission intensity was found to increase with dendritic pendants upon thermal annealing, which is ascribed to energetically favored stacking of dendritic pendants that suppresses interchromophoric quenching between fluorene units. Relative to 9,10-

diphenylanthracene in a poly(methyl-methacrylate) film at  $10^{-2}$  M, the fluorescence quantum yield was found to decrease from 0.28 to 0.24 with phenyl pendants but to increase from 0.16 to 0.24 with dendritic pendants as a result of prolonged heating.

## EXPERIMENTAL SECTION

**Materials.** All chemicals, reagents and solvents were used as received from commercial sources without further purification except tetrahydrofuran (THF) and toluene that had been distilled over sodium/benzophenone and sodium, respectively. Intermediates 3, 6-diphenylphthalyl alcohol (**2**), 1, 2-bis(hydroxymethyl)-3, 4, 5, 6-tetraphenylbenzene (**3**), and 2, 2', 7, 7'-tetrabromo-9, 9'-spirobifluorene (**8**) were all synthesized following literature procedures [33].

**2', 3'-bis (bromomethyl)-*p*-terphenyl (**4b**).** Into a solution of **2** (12.5 g, 43.2 mmol) and  $\text{CBr}_4$  (35.8 g, 0.107 mol) in anhydrous THF (80 ml) was added  $\text{PPh}_3$  (28.3 g, 0.108 mmol) in two portions. The resultant mixture was stirred for 30 min before adding a large amount of water. The mixture was extracted with methylene chloride. The organic extracts were washed with brine and dried over anhydrous  $\text{MgSO}_4$ . The solvent was removed by evaporation to produce a white solid. Further purification was accomplished by column chromatography on silica gel with petroleum ether: methylene chloride (4:1) as the eluent to yield 13.9 g (77 %).  $^1\text{H-NMR}$  ( $\text{CDCl}_3$ , 400 MHz):  $\delta$  7.40–7.60 (m, Ph-H, 10 H), 7.30–7.40 (m, Ph-H, 2 H), 4.70–4.90 (m,  $-\text{CH}_2-$ , 4 H).

**1, 2-bis (bromomethyl)-3, 4, 5, 6-tetraphenylbenzol (**4c**).** The same procedures described for the synthesis and purification of **4b** were followed to produce **4c** as a white solid in 87 % yield.

<sup>1</sup>H-NMR (CDCl<sub>3</sub>): δ 7.10–7.24 (m, Ph-H, 10 H), 6.70–6.90 (m, Ph-H, 10 H), 4.66 (s, -CH<sub>2</sub>-, 4 H). <sup>13</sup>C-NMR (CDCl<sub>3</sub>): δ 142.81, 142.46, 139.50, 138.60, 134.30, 130.71, 130.05, 127.42, 126.85, 125.50, 29.66.

**Spiro (2-bromo-fluorene-9, 2'-indane) (6a).** Into a solution of 2-bromofluorene (**5**, 3.0 g, 12.2 mmol) and α, α'-dibromomethylbenzene (**4a**, 3.24 g, 12.2 mmol) in toluene (20 ml) was added a 50 wt % NaOH aqueous solution (10 ml) followed by benzyltriethylammonium chloride (140 mg, 0.614 mmol) as a phase transfer catalyst. The reaction mixture was vigorously stirred overnight and then poured into 200 ml water for extraction with methylene chloride. The combined organic extracts were washed with brine before drying over anhydrous MgSO<sub>4</sub>. Upon evaporating off the solvent, the solid residue was purified by column chromatography on silica gel with petroleum ether as the eluent to yield a white solid product in 2.14 g (50 %). <sup>1</sup>H-NMR (CDCl<sub>3</sub>): δ 7.73 (dd, fluorenyl-H, 1 H), 7.62 (d and broad, fluorenyl-H, 1 H), 7.49 (dd, fluorenyl-H, 1 H), 7.30–7.43 (m, Ar-H, 2 H), 7.22–7.28 (m, Ar-H, 6 H), 3.46 (m, -CH<sub>2</sub>-, 4 H). <sup>13</sup>C-NMR (CDCl<sub>3</sub>): δ 154.54, 152.10, 142.34, 138.61, 138.54, 130.47, 127.96, 127.53, 127.01, 125.73, 124.77, 122.42, 121.16, 119.86, 57.41, 45.21.

**Spiro (2-bromo-fluorene-9, 2'-(4', 7'-diphenyl indane)) (6b).** Into a solution of **5** (2.36 g, 9.63 mmol) and **4b** (4.0 g, 9.61 mmol) in toluene (70 ml) was added 50 wt % NaOH solution (35 ml) followed by benzyltriethylammonium chloride (110 mg, 0.483 mmol) as a phase transfer catalyst. The reaction mixture was vigorously stirred for 5 h when an additional amount of **5** (0.90 g, 3.92 mmol) was added. The reaction was allowed to continue till **4b** was completely consumed as monitored by thin layer chromatography. The reaction mixture was then shaken

with water (200 ml) and methylene chloride (200 ml). The organic phase was separated, and the aqueous phase was extracted with methylene chloride. The combined organic extracts were washed with brine and dried over anhydrous  $\text{MgSO}_4$ . Upon evaporating off the solvent, the solid residue was washed with a large amount of acetone to yield **6b** as a white solid product in 2.66 g. After evaporating off acetone, the solid residue was further purified on a silica gel column with petroleum ether:methylene chloride (4:1) as the eluent, yielding additional 0.45 g of **6b**; the total yield was 65%.  $^1\text{H-NMR}$  ( $\text{CDCl}_3$ ):  $\delta$  7.65 (d, fluorenyl-H, 1 H), 7.28–7.58 (m, Ar-H, 16 H), 7.18–7.24 (m, Ar-H, 2 H), 3.66 (d,  $-\text{CH}_2-$ , 2 H), 3.54 (d,  $-\text{CH}_2-$ , 2 H).  $^{13}\text{C-NMR}$  ( $\text{CDCl}_3$ ):  $\delta$  153.73, 151.96, 140.76, 140.58, 138.80, 138.47, 137.74, 130.55, 128.55, 128.41, 128.17, 127.97, 127.58, 127.17, 125.85, 122.23, 121.22, 119.99, 57.66, 45.27.

**Spiro (2-bromo-fluorene-9, 2'-(4', 5, 6, 7'-tetraphenyl indane)) (6c).** The procedures described above for the synthesis and purification of **6b** were followed to produce **6c** in 2.32 g (58 %).  $^1\text{H-NMR}$  ( $\text{CDCl}_3$ ):  $\delta$  7.60–7.70 (m, fluorenyl-H, 2 H), 7.55 (d, fluorenyl-H, 1 H), 7.42–7.48 (m, fluorenyl-H, 2 H), 7.29–7.38 (m, fluorenyl-H, 3 H), 7.0–7.20 (m, Ph-H, 10 H), 6.80–7.00 (m, Ph-H, 10 H), 3.47 (d,  $-\text{CH}_2-$ , 2 H), 3.36 (d,  $-\text{CH}_2-$ , 2 H).  $^{13}\text{C NMR}$  ( $\text{CDCl}_3$ ):  $\delta$  154.36, 152.72, 140.25, 140.10, 139.97, 139.90, 138.68, 138.30, 137.64, 131.58, 131.50, 130.33, 129.78, 128.00, 127.52, 127.40, 126.60, 126.09, 125.80, 125.30, 122.14, 121.13, 121.08, 119.77, 56.68, 45.72.

**General procedure for the preparation of 7.** Into a solution of **6** in anhydrous THF was slowly added *n*-BuLi (1.2 equiv.) at  $-78^\circ\text{C}$ , where the reaction mixture was stirred for 1 h before adding triisopropyl borate (for **7a** and **7c**) and 2-isopropyl-4,4,5,5-tetramethyl-1,3,2-

dioxaborolane (for **7b**) at 1.5 equivalents in all cases. The reaction mixture was allowed to warm up to room temperature and then stirred overnight. With triisopropyl borate as the reagent, 2.0 N HCl (10 equiv.) was added to quench the reaction. In both cases, the reaction mixture was mixed with a large amount of water for extraction with ether. The organic extracts were washed with brine before drying over anhydrous  $\text{MgSO}_4$ . Upon evaporating off the solvent, the crude products of **7a** and **7c** were washed with hexane several times. The crude product of **7b** was purified by column chromatography on silica gel with methylene chloride as the eluent.

**7a:** Yield: 89 %, white powder.  $^1\text{H}$  NMR ( $\text{CDCl}_3$ ):  $\delta$  7.60–8.16 (m, fluorenyl-H, 4 H), 7.28–7.45 (m, Ar-H, 4 H), 7.21–7.28 (m, Ar-H, 3 H), 3.25–3.75 (m,  $-\text{CH}_2-$ , 4 H).

**7b:** Yield: 79 %, white powder.  $^1\text{H}$  NMR ( $\text{CDCl}_3$ )  $\delta$  8.10 (s, fluorenyl-H, 1 H), 7.83 (d, fluorenyl-H, 1 H), 7.70 (dd, fluorenyl-H, 2 H), 7.47–7.53 (m, Ar-H, 6 H), 7.35–7.41 (m, Ar-H, 4 H), 7.20–7.32 (m, Ar-H, 3 H), 7.00–7.10 (m, Ar-H, 1 H), 6.95 (d, Ar-H, 1 H), 4.0 (d,  $-\text{CH}_2-$ , 2 H), 3.28 (d,  $-\text{CH}_2-$ , 2 H), 1.40 (s,  $\text{CH}_3$ , 12 H).

**7c:** Yield: 80 %, white powder.  $^1\text{H}$  NMR ( $\text{CDCl}_3$ ):  $\delta$  8.28–8.40 (m, fluorenyl-H, 1 H), 7.25–8.00 (m, fluorenyl-H, 6 H), 6.85–7.20 (m, Ph-H, 20 H), 3.25–3.75 (m,  $-\text{CH}_2-$ , 4 H).

**General procedure for the Suzuki coupling.** To a Shlenck tube containing **8** (1 equivalent), **7** (5 to 6 equivalents), and  $\text{Pd}(\text{PPh}_3)_4$  (8 mol %) was added toluene and a 2.0 M aqueous solution of  $\text{Na}_2\text{CO}_3$  (50 equivalents; toluene:water at 6:4). The reaction mixture was stirred vigorously at 90  $^\circ\text{C}$  for 2 days followed by the addition of a large amount of methylene chloride. The organic

phase was separated and washed with brine before drying over anhydrous  $\text{MgSO}_4$ . Upon evaporating off the solvent, crude products of **1a** and **1c** were purified by column chromatography on silica gel with petroleum ether: methylene chloride (2:1) as the eluent. The crude product of **1b** could not be purified by column chromatography because of limited solubility. Instead, it was washed repeatedly with toluene. All three final products were obtained in white powders via precipitation from a chloroform solution into methanol followed by thorough drying.

**1a:** Yield, 71 %.  $^1\text{H}$ -NMR ( $\text{CDCl}_3$ , 400 MHz):  $\delta$  7.93 (d,  $\text{H}_a$ , 4 H), 7.66–7.71 (m,  $\text{H}_{d,e}$ , 8 H), 7.63 (dd,  $\text{H}_b$ , 4H), 7.47 (dd,  $\text{H}_f$ , 4 H), 7.10–7.40 (m,  $\text{H}_{g,h,i,j}$  and Ph-H, 32 H), 6.94 (d,  $\text{H}_c$ , 4 H), 3.45 (d,  $\text{H}_k$ , 8 H). 3.34 (d,  $\text{H}_k$ , 8 H).  $^{13}\text{C}$  NMR ( $\text{CDCl}_3$ , 100 MHz):  $\delta$  152.81, 152.53, 149.64, 142.72, 140.89, 140.59, 140.11, 139.03, 138.80, 127.38, 127.28, 126.90, 126.73, 126.41, 124.58, 122.51, 122.10, 120.90, 120.32, 119.88, 119.76, 66.12, 57.46, 45.22. Anal. Calcd. for  $\text{C}_{109}\text{H}_{72}$ : C, 94.75; H, 5.25. Found: C, 94.41; H: 5.30.

**1b:** Yield, 39 %.  $^1\text{H}$ -NMR ( $\text{CDCl}_3$ , 400 MHz):  $\delta$  8.16 (d,  $\text{H}_a$ , 4 H), 7.89 (dd,  $\text{H}_b$ , 4 H), 7.60–7.70 (m,  $\text{H}_{d,e,f}$ , 12 H), 7.00–7.36 (m,  $\text{H}_{g,h,i,j}$  and Ph-H, 64 H), 6.94 (d,  $\text{H}_c$ , 4 H), 3.62 (d,  $\text{H}_k$ , 8 H), 3.34 (d,  $\text{H}_k$ , 8 H).  $^{13}\text{C}$  NMR spectrum was not available because of its limited solubility. Anal. Calcd. for  $\text{C}_{157}\text{H}_{104}$ : C, 94.73; H, 5.27. Found: C, 94.47; H, 5.37.

**1c:** Yield, 61 %.  $^1\text{H}$ -NMR ( $\text{CDCl}_3$ , 400 MHz):  $\delta$  8.05 (d,  $\text{H}_a$ , 4H), 7.75 (dd,  $\text{H}_b$ , 4 H), 7.55–7.80 (m,  $\text{H}_{d,e,f}$ , 12 H), 7.20–7.50 (m,  $\text{H}_{g,h,i,j}$ , 16 H), 7.14 (d,  $\text{H}_c$ , 4 H), 6.80–7.05 (m, Ph-H, 80 H), 3.60 (d,  $\text{H}_k$ , 8 H), 3.20 (d,  $\text{H}_k$ , 8 H).  $^{13}\text{C}$ -NMR ( $\text{CDCl}_3$ , 100 MHz):  $\delta$  154.05, 152.01, 149.84,



140.99, 140.73, 140.20, 140.05, 139.95, 139.74, 139.10, 138.75, 137.59, 131.63, 131.57, 129.81, 127.60, 127.47, 127.24, 127.06, 126.66, 126.60, 126.01, 125.27, 122.55, 121.76, 120.98, 120.56, 119.95, 119.76, 66.43, 56.74, 45.82. Anal. Calcd. for  $C_{205}H_{136}$ : C, 94.73; H, 5.27. Found: C, 94.43; H, 5.14

**Molecular structures, morphology, and thermal transition temperatures.**  $^1H$ - and  $^{13}C$ -NMR spectra in  $CDCl_3$  were acquired with an Avance-400 spectrometer (400 MHz). Elemental analysis was carried out by Galbraith Laboratories, Inc. Single crystals of **6a**, prepared by slow evaporation of a chloroform solution in a methanol environment, were analyzed with a CCD X-ray diffractometer (Siemens SMART). Thermal transition temperatures were determined by DSC (Perkin-Elmer DSC-7) with a continuous  $N_2$  purge at 20 mL/min. Samples were preheated to beyond crystalline melting points followed by cooling at  $-20^\circ C/min$  to  $-30^\circ C$  before taking the reported second heating scans at  $20^\circ C/min$ . Morphology and the nature of phase transition were characterized with a polarizing optical microscope (DMLM, Leica, FP90 central processor and FP82 hot stage, Mettler Toledo). The absence of crystallites was further validated with electron diffractometry (see below).

**Film preparation and characterization.** Thin films on the order of 100 nm thick were prepared by spin-coating from 1.0 wt% solutions in chloroform at 5000 rpm on optically flat, fused silica substrates (25.4 mm diameter  $\times$  3 mm thick, Esco Products; transparent down to 200 nm) followed by vacuum drying at room temperature overnight. Film thickness was determined with a variable angle spectroscopic ellipsometer (VASE, J. A. Woollam, Corp., Inc.). A spectrophotometer (Lambda-900, Perkin-Elmer) was employed to gather UV-Vis absorption

spectra of thin films and in dilute solution. Photoluminescence was characterized with a spectrofluorimeter (Quanta Master C-60SE, Photon Technology International). The dilute solution spectra were taken in a 90° arrangement between excitation and detection beams. In the case of solid films, a straight-through arrangement was adopted in which a liquid light guide (Photon Technology International) was used to direct an excitation beam at 350 nm onto the center of the film; the light guide also served as a polarization randomizer. A glass filter (UG11, Corning) with an extinction factor of 5 optical density units at  $\lambda \geq 400$  nm was inserted in front of the film to prevent emitted light from reaching the detector. Thin films for electron diffraction were prepared following the same procedures except on NaCl substrates and then floated off in a trough filled with deionized water for mounting onto copper grids. Electron diffraction was performed on a transmission electron microscope (JEM 2000 EX, JEOL USA).

**Molecular simulation.** Molecular mechanics calculations were performed using the Amber software package with the Alchemy force-field parameters. The potential energy to be minimized accounts for all the interactions between bonded and nonbonded atoms in the system. Molecules of the three terfluorenes were divided into five fragments, the spiro-configured bifluorene core plus four fluorene units spiro-linked to aromatic groups. Molecular mechanics simulation was first carried out for these two types of structural fragment. The target molecule was then constructed by assigning an initial value of the torsion angle between the energy-minimized fragments. Systems of a single molecule and of a stack of two and three molecules were simulated, yielding molecular structures independent of the input torsion angle and the number of molecules in the simulation system.

**Measurement of fluorescence quantum yield.** As the primary standard for fluorescence quantum yield ( $\eta$ ), 9,10-diphenylanthracene (99%, Acros Organics) was repeatedly recrystallized from xylenes until pale yellow prism crystals were obtained. Anthracene (99%, Aldrich Chemical Company) was recrystallized from ethanol. Poly(methylmethacrylate) (PMMA, Polysciences, Inc.) with a weight-average molecular weight of 75,000 was used without further purification. About 5  $\mu\text{m}$  thick PMMA films doped with 9,10-diphenylanthracene and anthracene at  $10^{-2}$  M were spin-cast on fused silica substrates followed by drying *in vacuo* overnight. The film lightly doped with 9,10-diphenylanthracene was assigned a widely accepted value,  $\eta=0.83$  [34]. The anthracene-containing film was characterized with the following formula [35]:

$$\frac{\eta_s}{\eta_r} = \frac{1 - 10^{-A_r}}{1 - 10^{-A_s}} \frac{\overline{B_s n_s^2}}{\overline{B_r n_r^2}} \quad (1)$$

where subscripts  $s$  and  $r$  refer to sample and reference, respectively,  $A$  denotes absorbance at the excitation wavelength,  $B$  is the integrated intensity across the entire emission spectrum, and  $\overline{n^2}$  is defined as follows:

$$\overline{n^2} \equiv \frac{\int I(\lambda) n^2(\lambda) d\lambda}{\int I(\lambda) d\lambda} \quad (2)$$

in which  $I(\lambda)$  stands for emission intensity, and the integration is performed over the entire emission spectrum. A variable angle spectroscopic ellipsometer (VASE, J. A. Woollam Corp., Inc.) was employed for the measurement of refractive index dispersion,  $n(\lambda)$ , of neat films of **1a** and **1c**. The accuracy of our measurements was validated with a spin-coated 550 nm thick PMMA film, whose refractive index profile in the 300-900 nm spectral range was found to agree with refractometric data [36] to within 0.003. The significant difference in the measured

refractive index between materials **1a** and **1c** in the neighborhood of 400 nm, as shown in Figure 6, can be attributed to the absorption coefficient. Material **1a** has an absorption coefficient twice that of **1c** mainly because of the higher number density of terfluorene segments in neat film. The real part of the dielectric function was calculated through a Kramers-Kronig integration of the imaginary part. Thus, the material with a higher absorption coefficient is expected to have a higher refractive index near its absorption band [37]. The fluorescence quantum yield was measured using the spectrofluorimeter described above with emission detected at 60° off-normal to prevent excitation light from entering the detector. The result for the anthracene-containing PMMA film,  $\eta=0.28\pm0.03$ , agrees with the reported value of 0.27 in benzene and ethanol [38], thus validating the experimental procedure.

## ACKNOWLEDGMENT

The authors wish to thank A. S. Kende of the Department of Chemistry, S. D. Jacobs and K. L. Marshall of the Laboratory for Laser Energetics, University of Rochester, for technical advice and helpful discussions. They are grateful for the financial support provided by the Multidisciplinary University Research Initiative, administered by the Army Research Office, under DAAD19-99-1-0206, the Defense University Research Instrumentation Program under DAAD19-00-1-0074, and the National Science Foundation under Grant CTS-9818234. Additional funding was provided by the Department of Energy Office of Inertial Confinement Fusion under Cooperative Agreement No. DE-FC03-92SF19460 with the Laboratory for Laser Energetics and the New York State Energy Research and Development Authority. The support of DOE does not constitute an endorsement by DOE of the views expressed in this article.

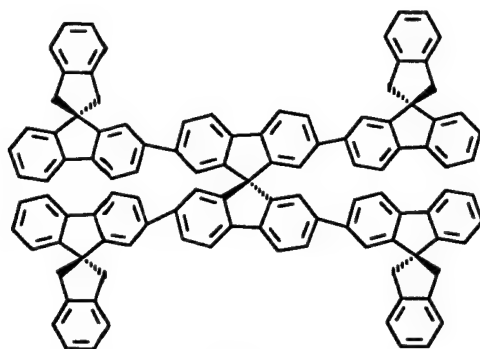
## REFERENCES

1. Salaneck, W. R.; Lundström, I.; Rånby, B., Eds. *Conjugated Polymers and Related Materials*; Oxford University Press: Oxford, 1993.
2. Friend, R. H.; Gymer, R. W.; Holmes, A. B.; Burroughes, J. H.; Marks, R. N.; Taliani, C.; Bradley, D. D. C.; Dos, Santos, D. A.; Brédas, J. L.; Lögdlund, M.; Salaneck, W. R. *Nature* **1990**, *347*, 539.
3. Tessler, N.; Denton, G. J.; Friend, R. H. *Nature* **1999**, *397*, 121.
4. Horowitz, G. *Adv. Mater.* **1998**, *10*, 365.
5. Bleir, H. In *Organic Materials for Photonics*; Zerbi, G., Ed.; Elsevier: Amsterdam, 1993; p.77.
6. Marder, S. R.; Kippelen, B.; Jen, A. K.-Y.; Peyghambarian, N. *Nature* **1997**, *388*, 845.
7. Nguyes, T.-Q.; Martini, I. B.; Liu, J.; Schwartz, J. J. *J. Phys. Chem. B* **2000**, *104*, 237.
8. Teetsov, J.; Vanden Bout, D. A. *J. Phys. Chem. B* **2000**, *104*, 9378.
9. Müllen, K.; Wegner, G. *Electronic Materials: The Oligomer Approach*; Wiley-VCH: Weinheim, New York, 1998.
10. Katsuma, K.; Shirota, Y. *Adv. Mater.* **1998**, *10*, 223.
11. Steuber, F.; Staudigel, J.; Stössel, M.; Simmerer, J.; Winnacker, A.; Spreitzer, H.; Weissörtel, F.; Salbeck, J. *Adv. Mater.* **2000**, *12*, 130.
12. Bach, U.; De Cloedt, K.; Spreitzer, H.; Grätzel, M. *Adv. Mater.* **2000**, *12*, 1060.
13. Wang, S.; Oldham, W. J.; Hudack, R. A., Jr.; Bazan, G. C. *J. Am. Chem. Soc.* **2000**, *122*, 5695.
14. Klärner, G.; Lee, J.-K.; Davey, M. H.; Miller, R. D. *Adv. Mater.* **1999**, *11*, 115.

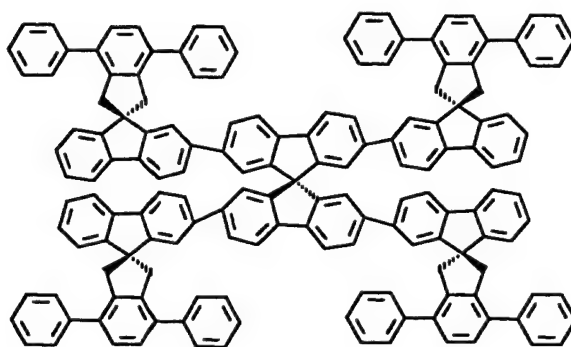
15. Yu, W.-L.; Pei, J.; Huang, W.; Heeger, A. J. *Adv. Mater.* **2000**, *12*, 828.
16. Virgili, T.; Lidzey, D. G.; Bradley, D. D. C. *Adv. Mater.* **2000**, *12*, 58.
17. Sainova, D.; Miteva, T.; Nothofer, H. G.; Scherf, U.; Glowaki, I.; Ulanski, J.; Fujikawa, H.; Neher, D. *Appl. Phys. Lett.* **2000**, *76*, 1810.
18. Weinfurter, K.-H.; Fujikawa, H.; Tokito, S.; Taga, Y. *Appl. Phys. Lett.* **2000**, *76*, 2502.
19. O'Brien, D. F.; Burrows, P. F.; Forrest, S. R.; Koene, B. E.; Loy, D. E.; Thompson, M. E. *Adv. Mater.* **1998**, *10*, 1108.
20. Johansson, N.; Salbeck, J.; Bauer, J.; Weissörtel, F.; Bröms, P.; Andersson, A.; Salaneck, W. R. *Adv. Mater.* **1998**, *10*, 1136.
21. Naito, K.; Miura, A. *J. Phys. Chem.* **1993**, *97*, 6240.
22. Jakubiak, R.; Collison, C. J.; Wan, W. C.; Rothberg, L. J.; Hsieh, B. R. *J. Phys. Chem. A* **1999**, *103*, 2394.
23. Bliznyuk, V. N.; Carter, S. A.; Scott, J. C.; Klärner, G.; Miller, R. D.; Miller, D. C. *Macromolecules*, **1999**, *32*, 361.
24. Jakubiak, R.; Bao, Z.; Rothberg, L. J. *Synth. Metals* **2000**, *114*, 61.
25. Setayesh, S.; Grimsdale, A. C.; Weil, T.; Enkelmann, V.; Müllen, K.; Meghdadi, F.; List, E. J. W.; Leising, G. *J. Am. Chem. Soc.* **2001**, *123*, 946.
26. Miyaura, N.; Suzuki, A. *Chem. Rev.* **1995**, *95*, 2457.
27. Schenk, H. *Acta. Cryst.* **1972**, *B28*, 625.
28. Belletête, M.; Ranger, M.; Beaupré, S.; Leclerc, M.; Durocher, G. *Chem. Phys. Lett.* **2000**, *316*, 101.
29. Klärner, G.; Davey, M. H.; Chen, W.-D.; Scott, J. C.; Miller, R. D. *Adv. Mater.* **1998**, *10*, 993.

30. Klärner, G.; Lee, J.-I.; Chan, F.; Chen, J.-P.; Nelson, A.; Markiewicz, D.; Siemens, R.; Scott, J. C.; Miller, R. D. *Chem. Mater.* **1999**, *11*, 1800.
31. Lee, J.-I.; Klärner, G.; Miller, R. D. *Chem. Mater.* **1999**, *11*, 1083.
32. Teetsov, J. A.; Vandan Bout, D. A. *J. Am. Chem. Soc.* **2001**, *123*, 3605.
33. (a) Abu-Yousef, I. A.; Hay, A. S. *Synth. Commun.* **1999**, *29*, 2915; (b) Smith, J. G.; Wikman, R. T. *Tetrahedron* **1974**, *30*, 2603; (c) Buchta, E.; Loew G. *Liebigs Ann.*, **1955**, 597, 123; (d) Bonner, E. F.; Finkensieper, A. G.; Becker, E. I., *J. Org. Chem.* **1953**, *18*, 426; (e) Wu, R. L.; Schumm, J. H.; Pearson, D. L.; Tour, J. M. *J. Org. Chem.* **1996**, *61*, 6906.
34. Melhuish, W. H. *J. Opt. Soc. Am.* **1964**, *54*, 183.
35. Demas, J. N.; Crosby, G. A. *J. Phys. Chem.* **1971**, *75*, 991.
36. Nikolov, I. D.; Ivanov, C. D. *Appl. Optics* **2000**, *39*, 2067.
37. Jellison, G. E., Jr.; Modine, F. A. *Appl. Phys. Lett.* **1996**, *69*, 371 and 2137.
38. Dawson, W. R.; Windsor, M. W. *J. Phys. Chem.* **1968**, *72*, 3251.

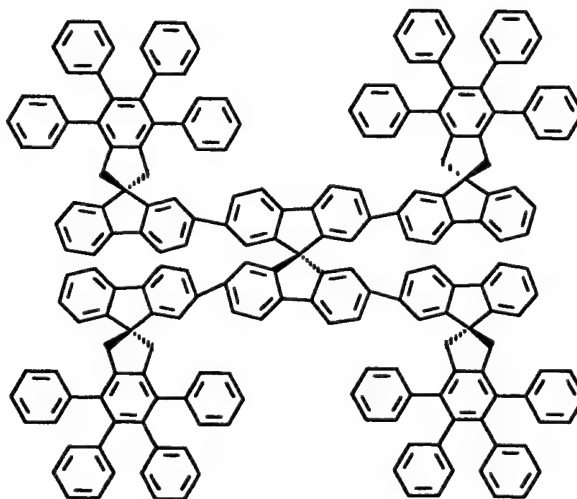
**Chart 1. Molecular structures of fully spiro-configured terfluorenes**



**1a**



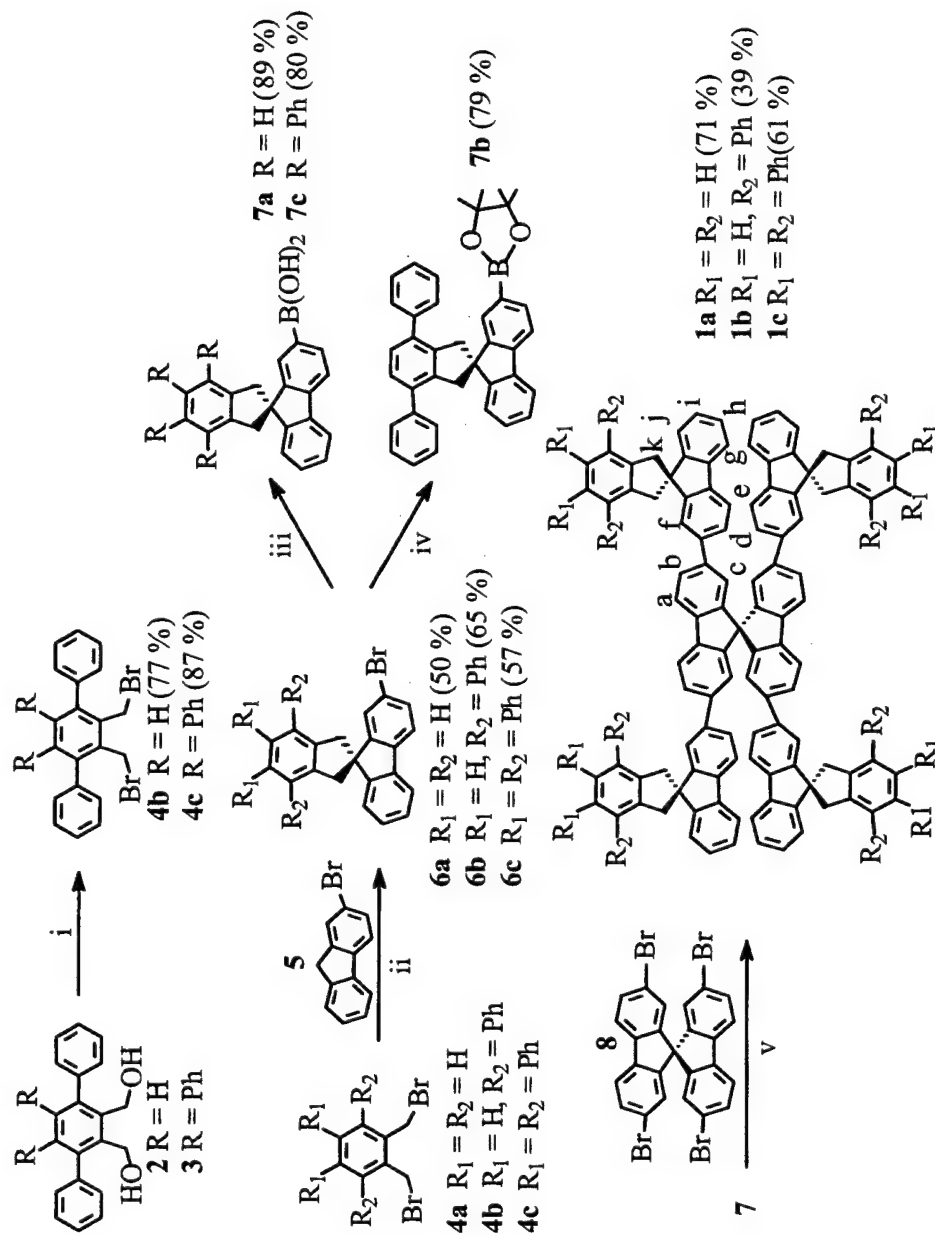
**1b**



**1c**



Scheme 1. Synthetic routes for fully spiro-configured terfluorenes 1a, b and c



- (i)  $CBBr_4$ ,  $PPh_3$ , THF, rt; (ii) NaOH (50 wt% aq.), PTC, DMSO, rt; (iii) 1)  $n-BuLi$ ,  $-78^\circ C$ , 2)  $(i-PrO)_3B$ ,  $-78^\circ C$  to rt, 3) HCl (2 M); (iv) 1)  $n-BuLi$ ,  $-78^\circ C$ , 2) 2-isopropoxy-4, 4, 5, 5-tetramethyl-1, 3, 2-dioxaborolane,  $-78^\circ C$  to rt, 3)  $H_2O$ ; (v)  $Pd(PPh_3)_4$ ,  $Na_2CO_3$  (2.0 M aq.), toluene,  $90^\circ C$ .

## FIGURE CAPTIONS

Figure 1.  $^1\text{H}$ -NMR spectrum ( $\text{CDCl}_3$ ) of terfluorene **1c**.

Figure 2.  $^{13}\text{C}$ -NMR spectrum ( $\text{CDCl}_3$ ) of terfluorene **1c**.

Figure 3. Crystal structure of **6a** based on X-ray analysis: monoclinic, space group  $C2/c$ ,  $a=20.3801(15)\text{ \AA}$ ,  $b=7.2207(5)\text{ \AA}$ ,  $c=21.7716(16)\text{ \AA}$ ,  $\alpha=90^\circ$ ,  $\beta=96.1220(10)^\circ$ ,  $\gamma=90^\circ$ ,  $V=3185.6(4)\text{ \AA}^3$ ,  $Z=8$ ,  $T=193(2)\text{ K}$ ; crystal size:  $0.20\text{ mm}\times 0.20\text{ mm}\times 0.40\text{ mm}$ .

Figure 4 (A) Molecular design concept for fully spiro-configured terfluorenes; (B) Molecular structures from molecular mechanics calculations using the Amber software package and the Alchemy force-field parameters.

Figure 5. Differential scanning calorimetric thermograms at  $+20\text{ }^\circ\text{C/min}$  of terfluorines **1a**, **1b**, and **1c** preheated to  $370$ ,  $480$ , and  $370\text{ }^\circ\text{C}$ , respectively, followed by cooling to  $-30\text{ }^\circ\text{C}$  at a rate of  $-200\text{ }^\circ\text{C/min}$ .

Figure 6. The effects of thermal annealing at  $100\text{ }^\circ\text{C}$  under argon for  $96\text{ h}$  on UV-Vis absorption and fluorescence (with  $350\text{ nm}$  photoexcitation) spectra of spin-coated films: (A) **1a**,  $76\text{ nm}$  thick; (B) **1c**,  $124\text{ nm}$  thick. The amorphous character of both films prior and subsequent to thermal annealing is revealed with electron diffraction patterns shown as insets; the refractive index dispersion,  $n(\lambda)$ , measured with variable angle spectroscopic ellipsometry is also included as insets.

Figure 1

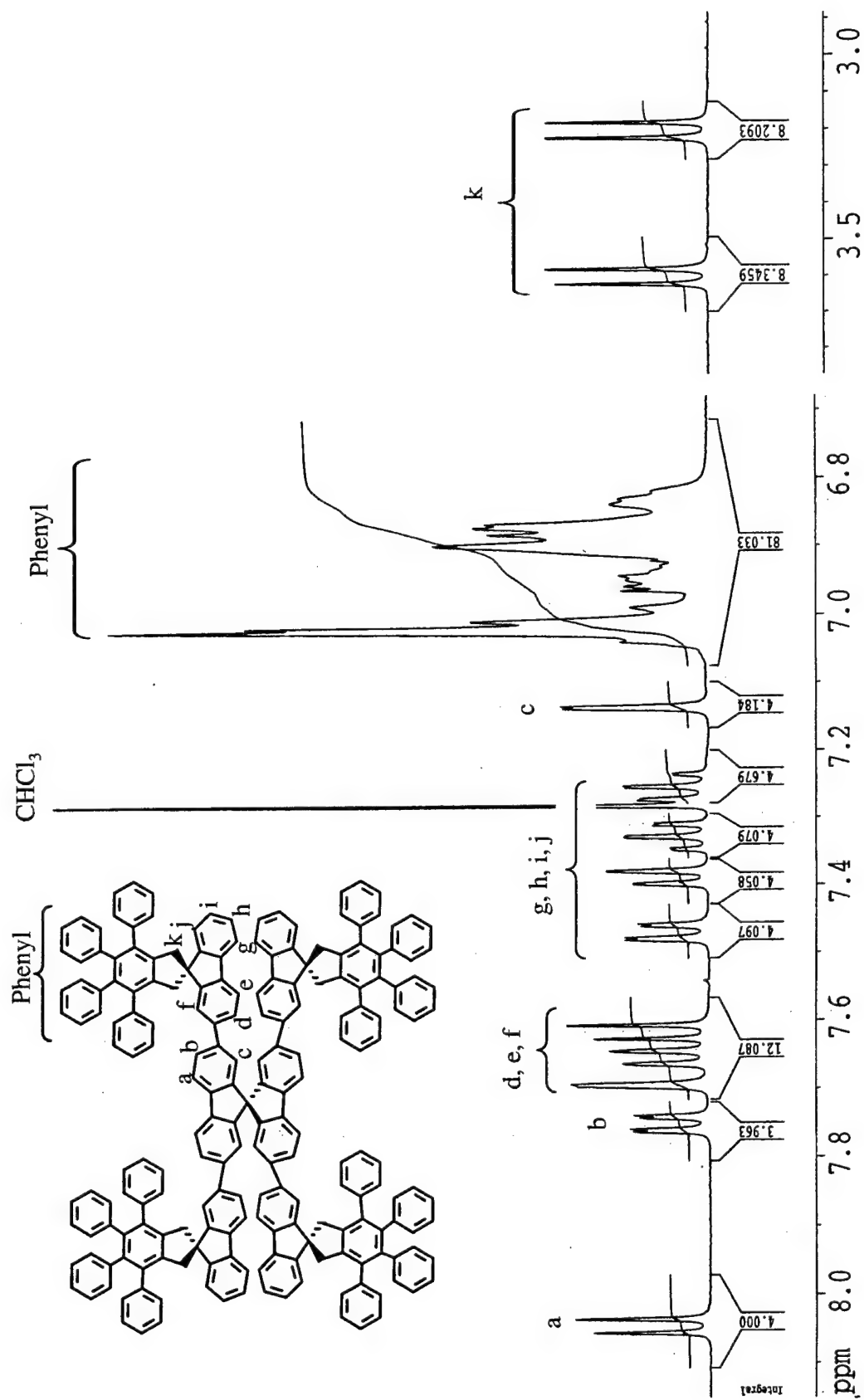


Figure 2

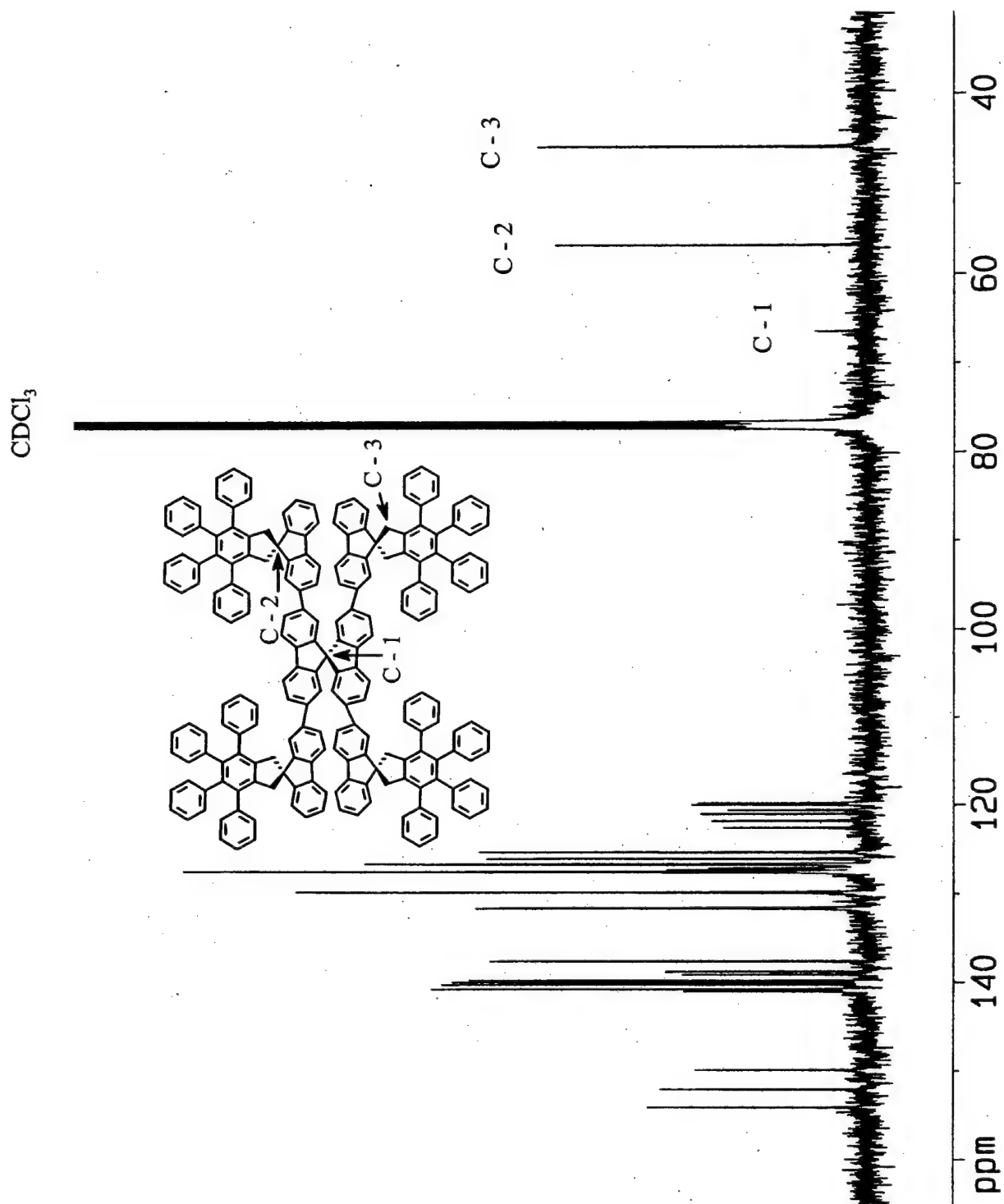


Figure 3

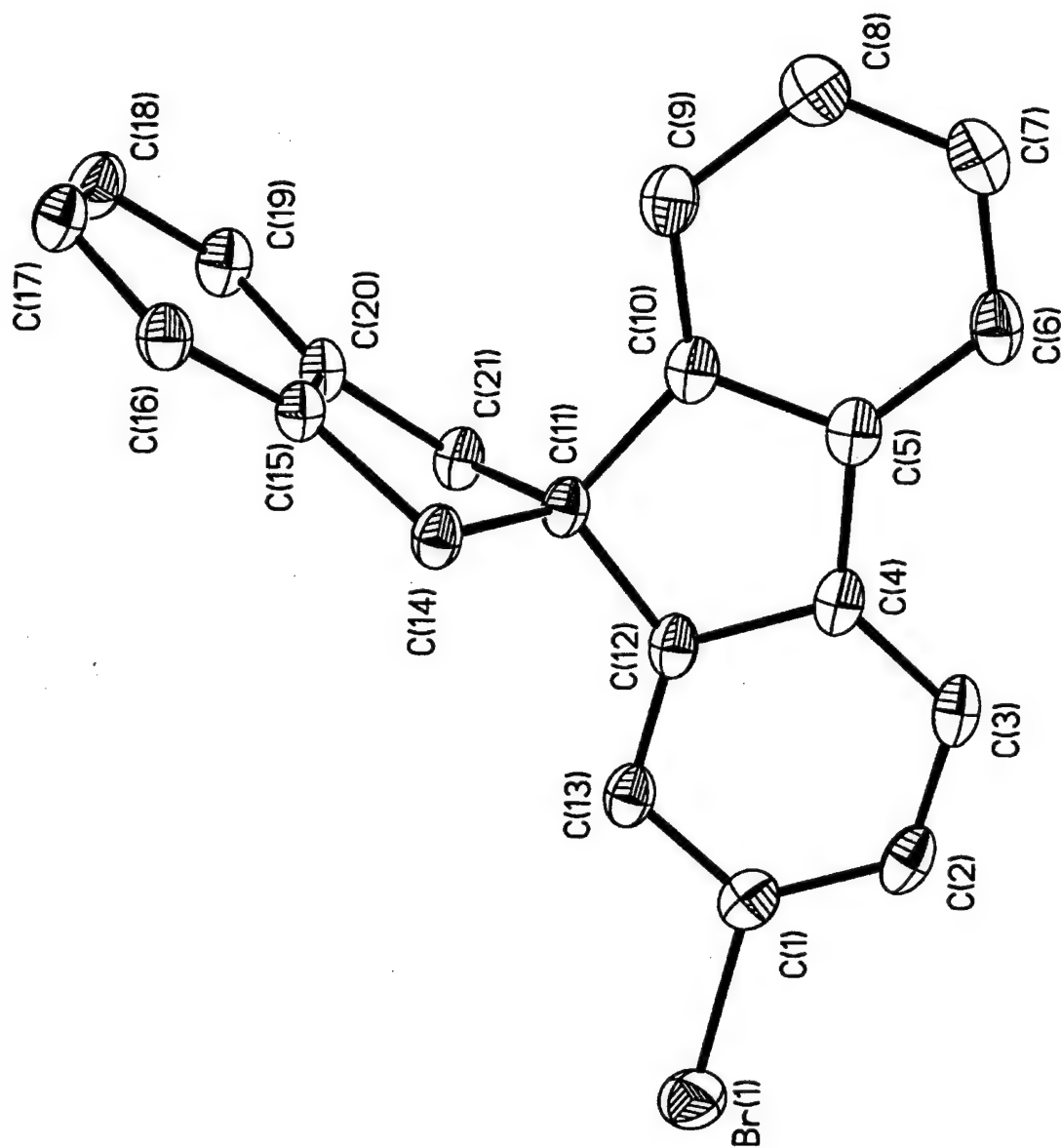
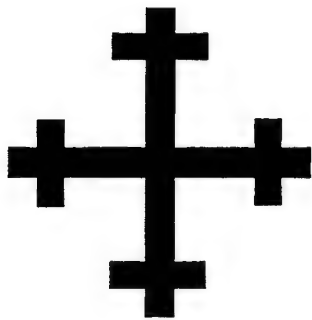


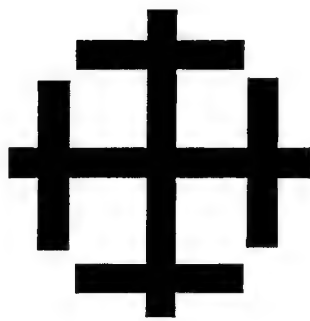
Figure 4

(A)

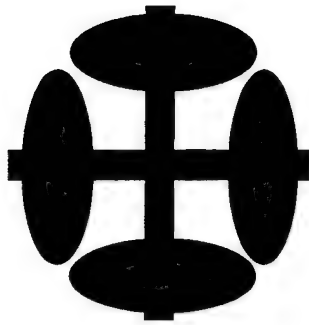
1a



1b



1c



(B)

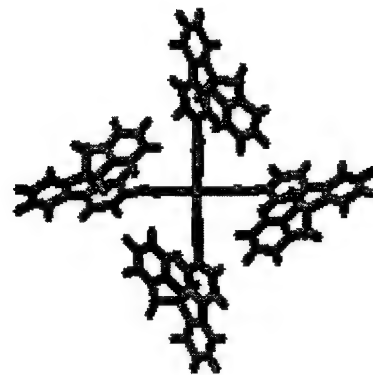
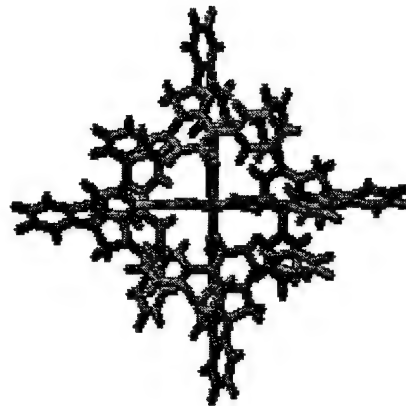
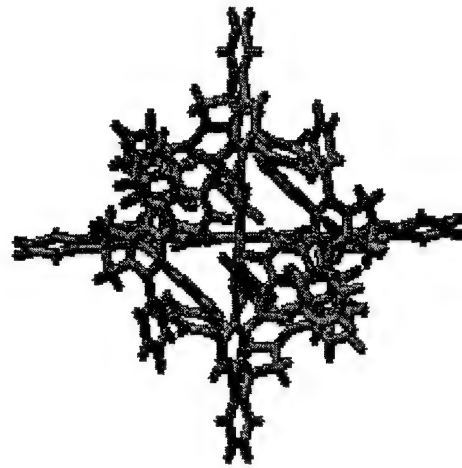


Figure 5

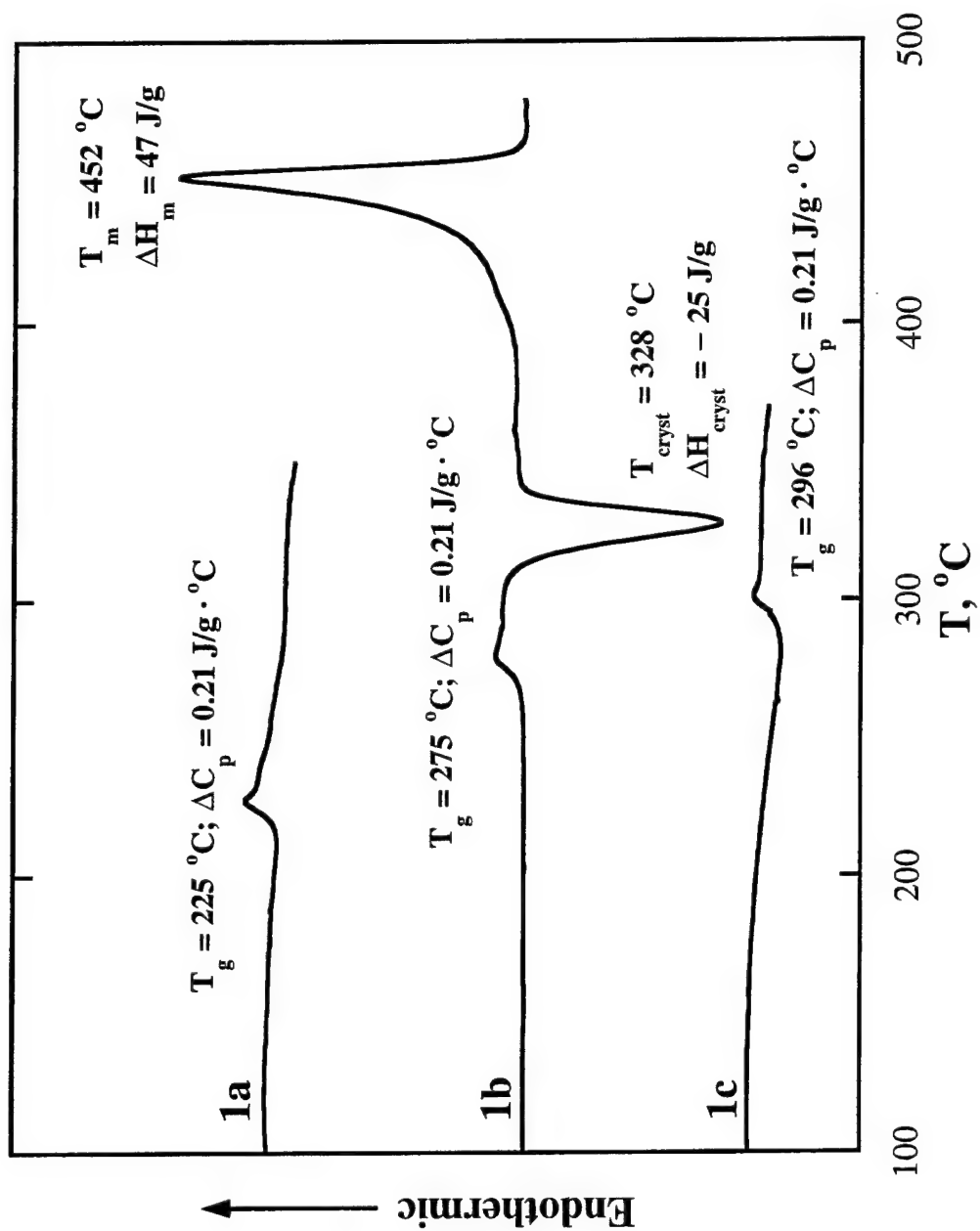
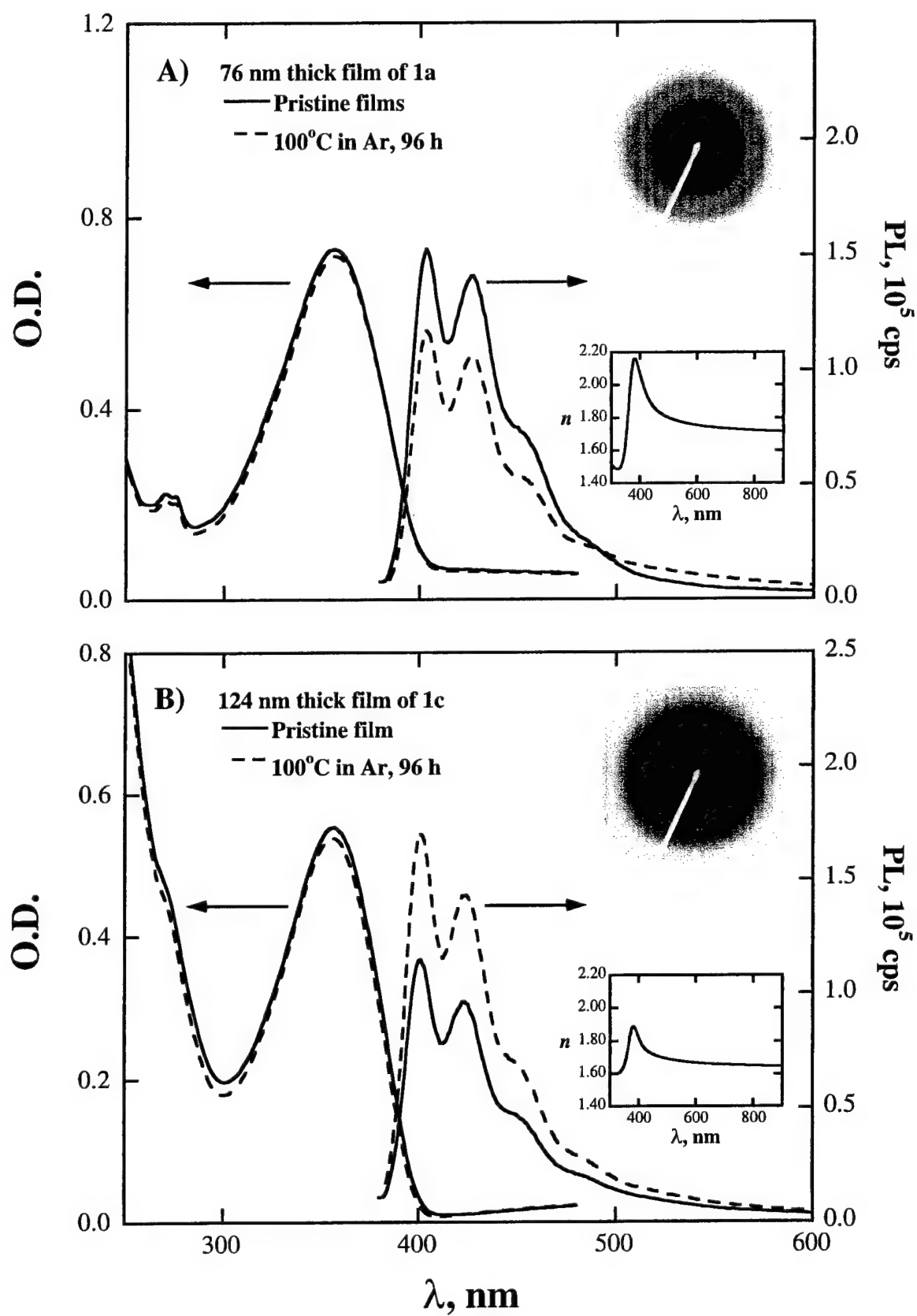


Figure 6





**Supporting Information Available:** Experimental section;  $^1\text{H}$ -NMR spectra of selected intermediates and target compounds **1a** and **1b**; UV-Vis absorption and fluorescence spectra in dilute chloroform solutions of **1a**, **1b**, and **1c**; X-ray crystallographic file for **6a**. This material is available free of charge via the Internet at <http://pubs.acs.org>.

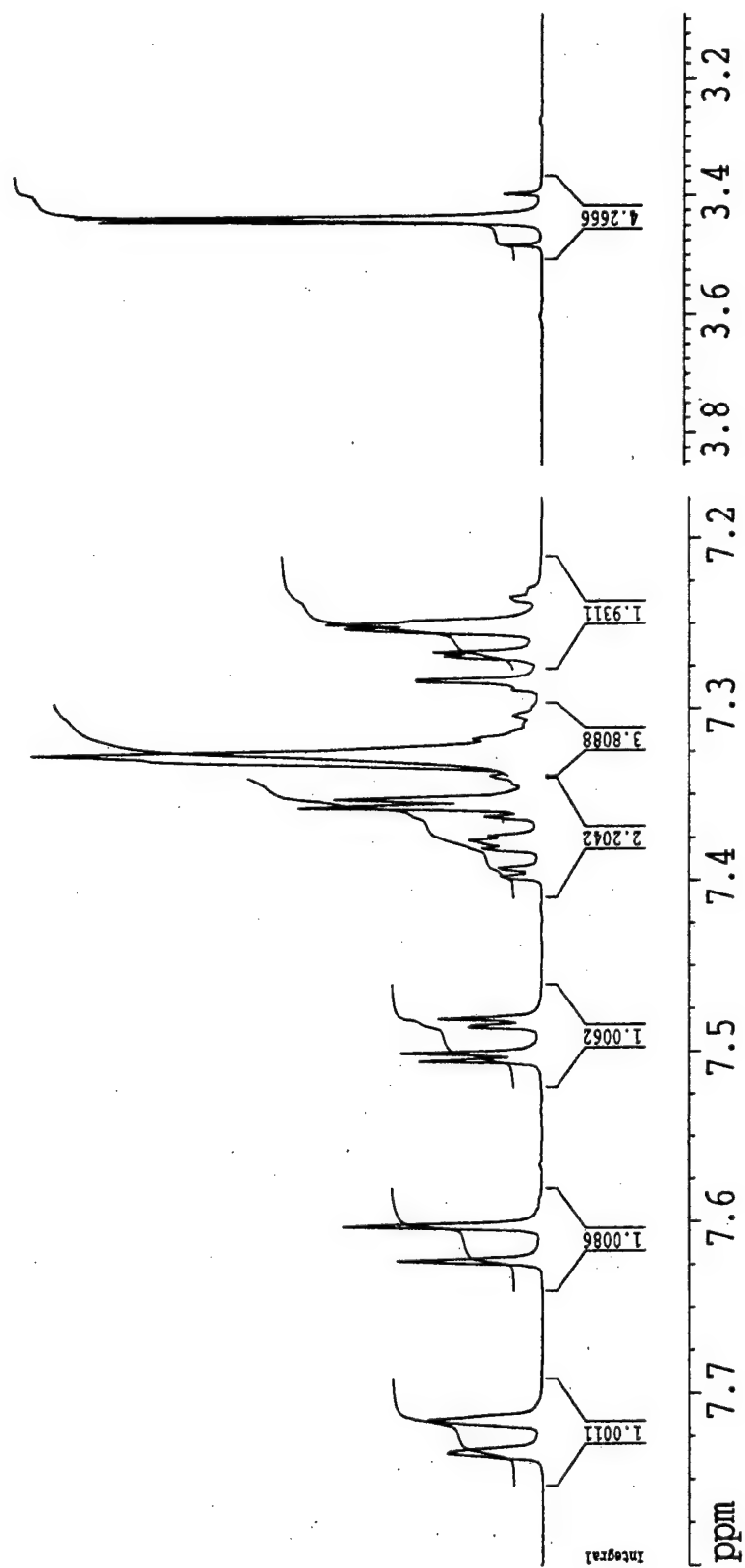


Figure S.1.1. Proton-NMR spectrum (CDCl<sub>3</sub>, 400MHz) of intermediate **6a**.

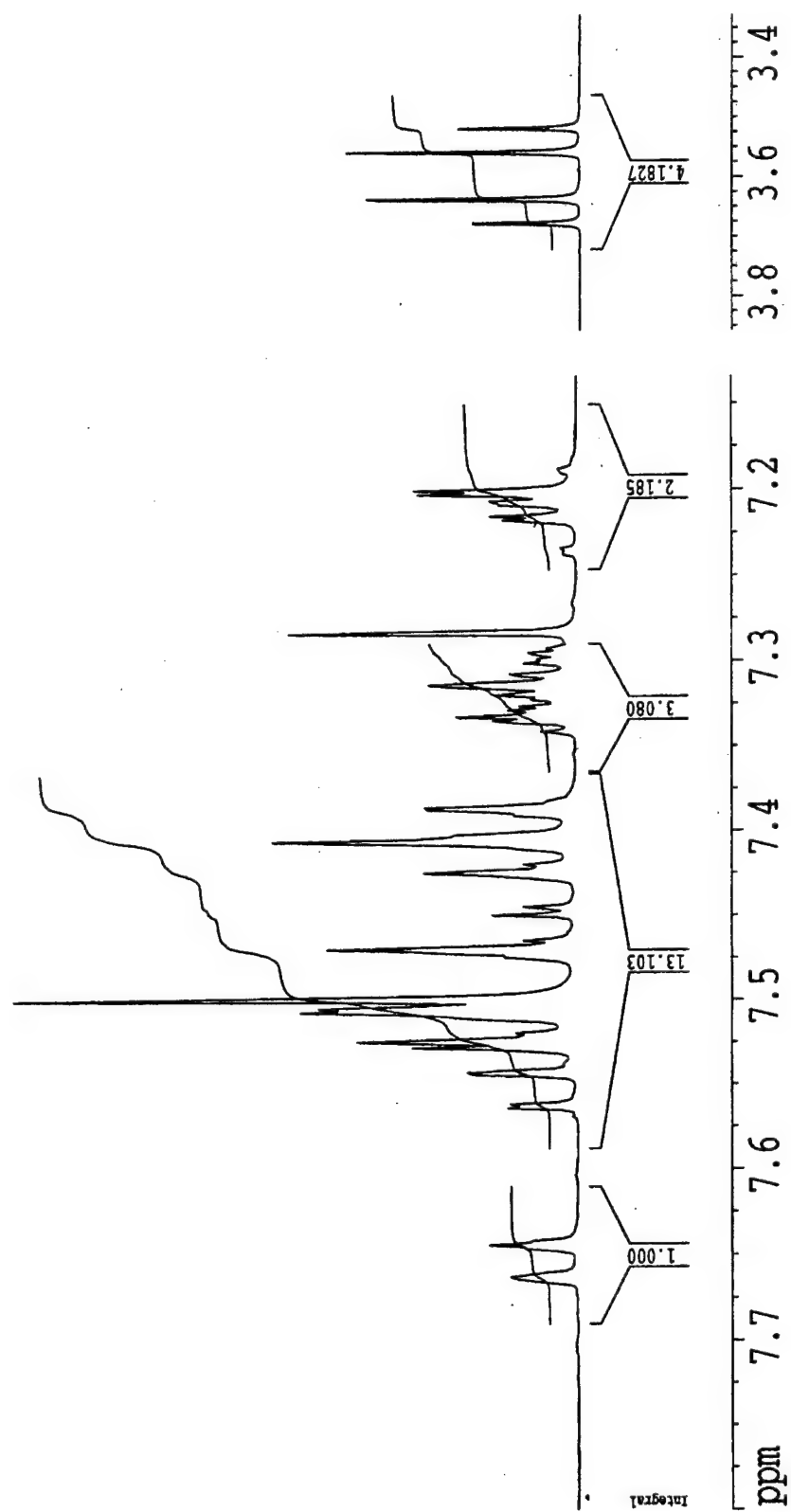


Figure S.2. Proton-NMR spectrum (CDCl<sub>3</sub>, 400MHz) of intermediate **6b**.

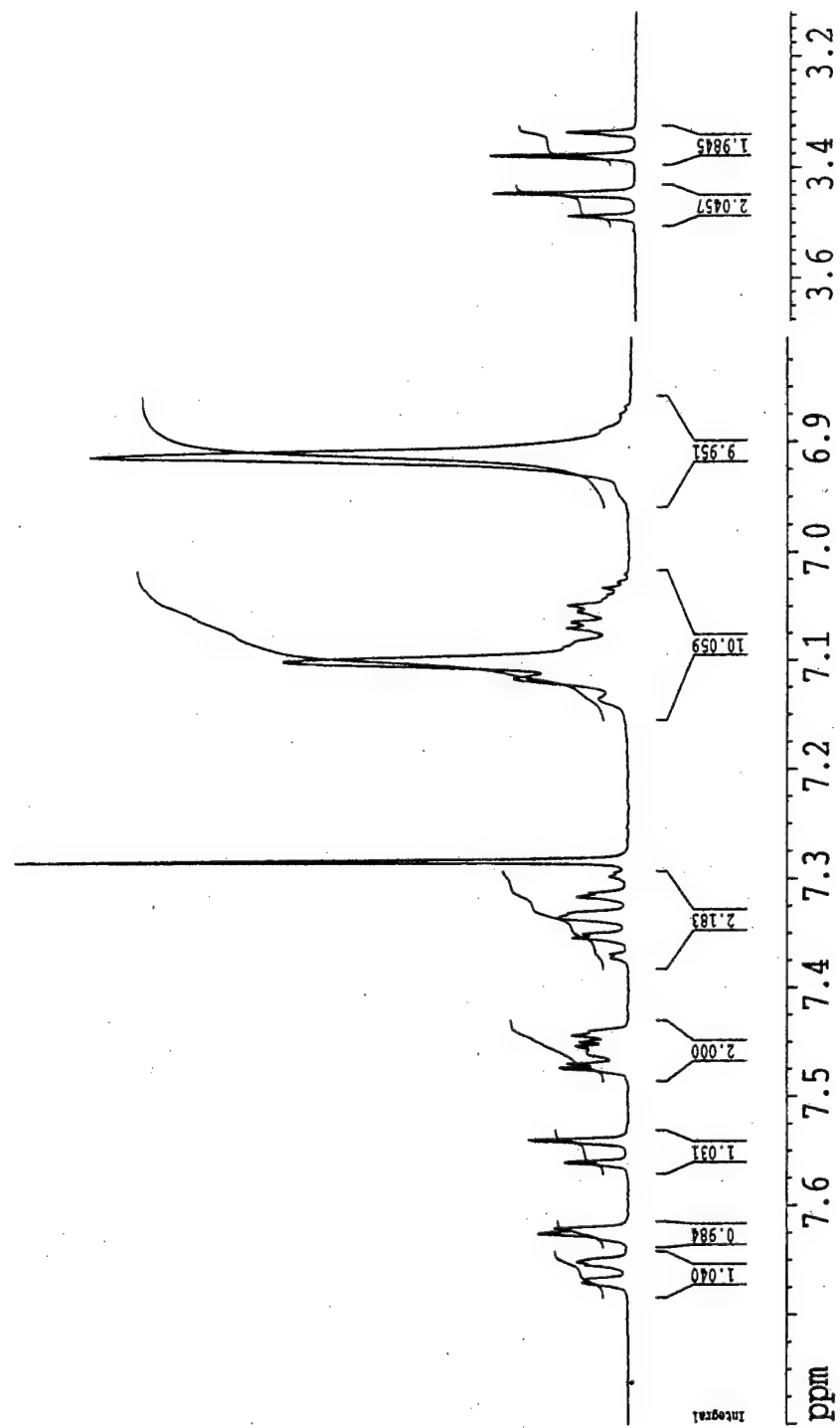


Figure S.3. Proton-NMR spectrum (CDCl<sub>3</sub>, 400MHz) of intermediate **6c**.

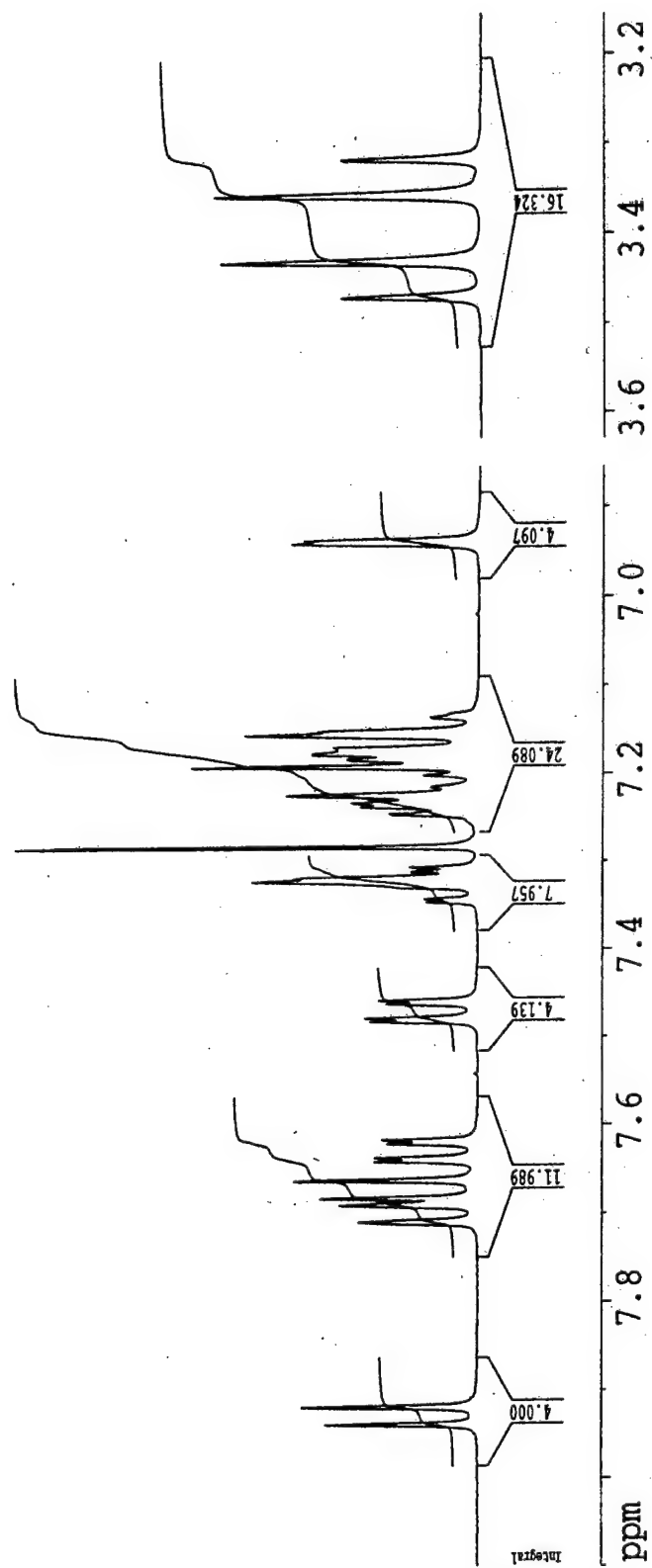


Figure S.4. Proton-NMR spectrum (CDCl<sub>3</sub>, 400MHz) of oligo(fluorene) **1a**.

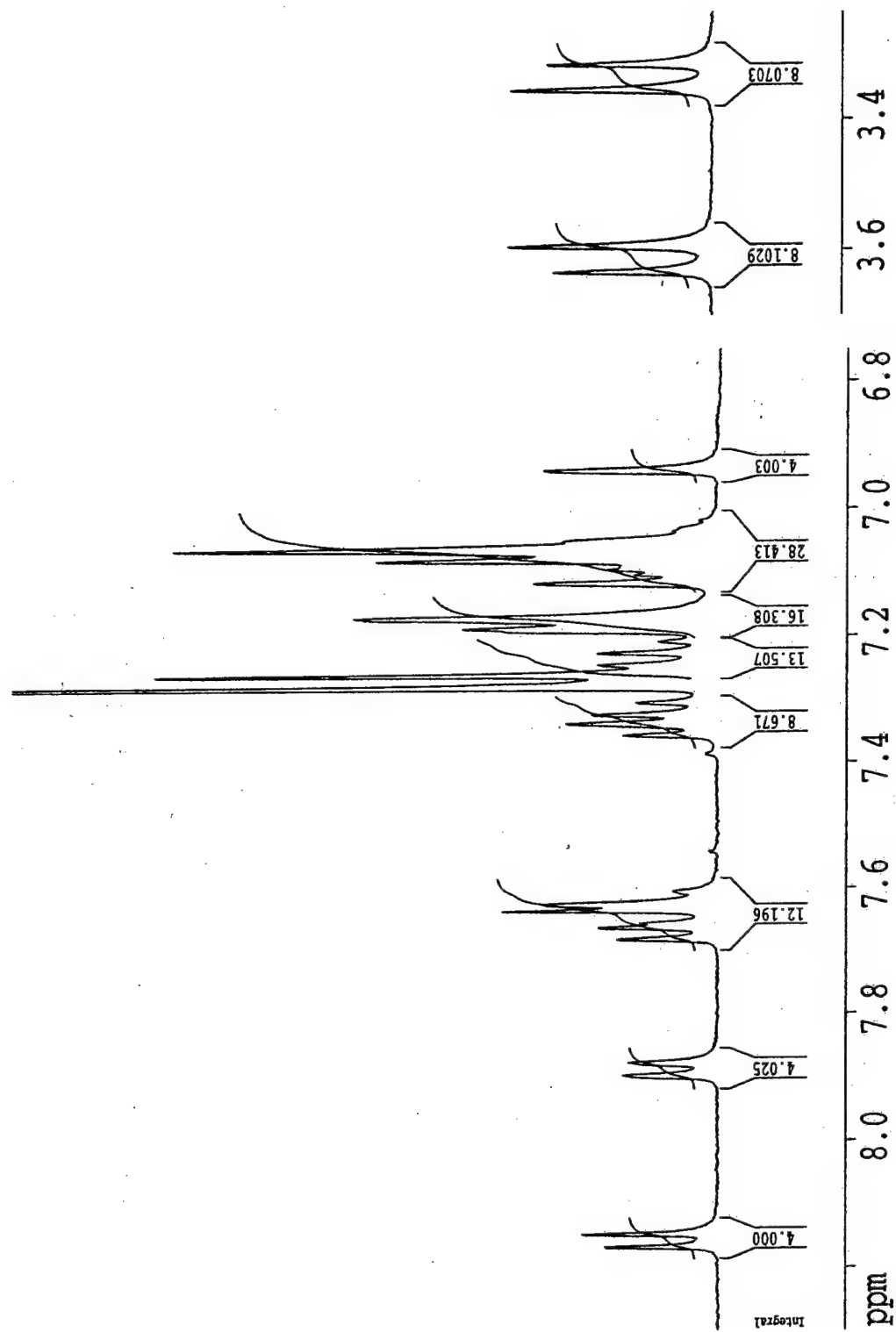


Figure S.5. Proton-NMR spectrum (CDCl<sub>3</sub>, 400MHz) of oligo(fluorene) **1b**.

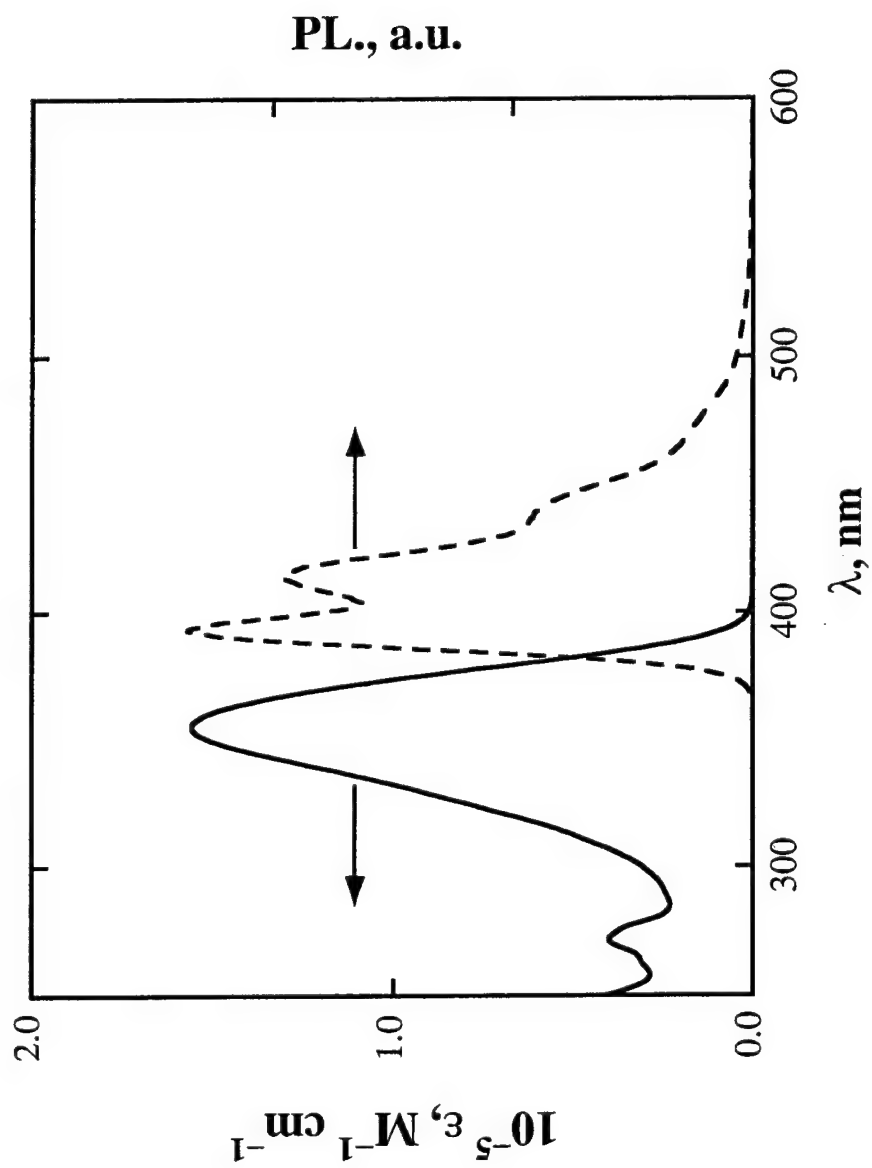


Figure S.6. Molar extinction coefficient,  $\epsilon$ , and fluorescence spectra with photoexcitation at 355 nm of **1a** at  $1.05 \times 10^{-5} \text{M}$  in chloroform.

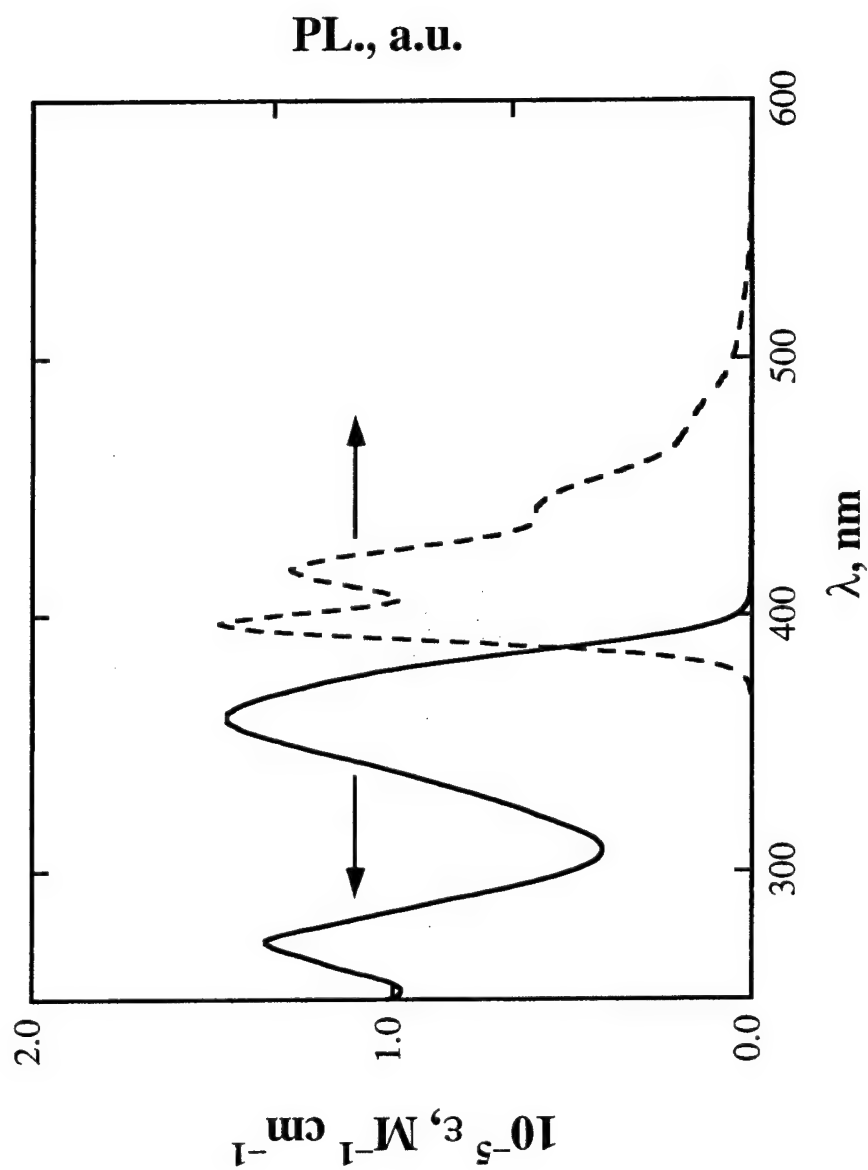


Figure S.7. Molar extinction coefficient,  $\epsilon$ , and fluorescence spectra with photoexcitation at 355 nm of **1b** at  $1.01 \times 10^{-5} \text{M}$  in chloroform.



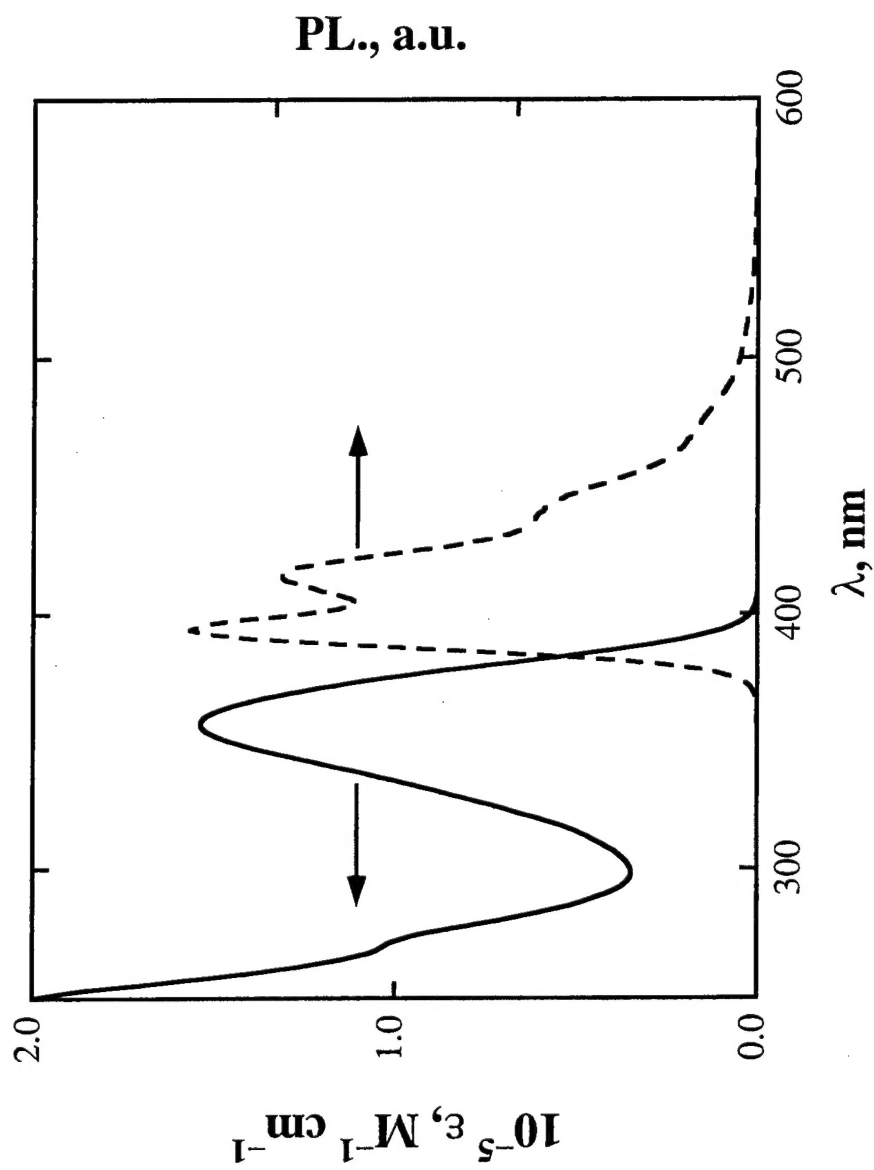


Figure S.8. Molar extinction coefficient,  $\epsilon$ , and fluorescence spectra with photoexcitation at 355 nm of **1c** at  $9.81 \times 10^{-6} \text{M}$  in chloroform.

Sad.tex

Table 1. Crystal data and structure refinement for sad.

Identification code	sad/chendgl
Empirical formula	C21 H15 Br
Formula weight	347.24
Temperature	193(2) K
Wavelength	0.71073 Å
Crystal system	Monoclinic
Space group	C2/c
Unit cell dimensions	a = 20.3801(15) Å    alpha = 90 deg. b = 7.2207(5) Å    beta = 96.1220(10) deg. c = 21.7716(16) Å    gamma = 90 deg.
Volume, Z	3185.6(4) Å <sup>3</sup> , 8
Density (calculated)	1.448 Mg/m <sup>3</sup>
Absorption coefficient	2.574 mm <sup>-1</sup>
F(000)	1408
Crystal size	0.20 x 0.20 x 0.40 mm
Theta range for data collection	1.88 to 23.26 deg.
Limiting indices	-22<=h<=22, -5<=k<=8, -23<=l<=24
Reflections collected	6505
Independent reflections	2246 [R(int) = 0.0200]
Reflections >2Sig(I)	1962
Absorption correction	SADABS
Max. and min. transmission	0.928 0.642
Refinement method	Full-matrix least-squares on F <sup>2</sup>
Data / restraints / parameters	2246 / 0 / 199
Goodness-of-fit on F <sup>2</sup>	1.167
Final R indices [I>2sigma(I)]	R1 = 0.0455, wR2 = 0.1045
R indices (all data)	R1 = 0.0560, wR2 = 0.1072
Largest diff. peak and hole	0.910 and -0.283 e.Å <sup>-3</sup>

Table 2. Atomic coordinates (x 10<sup>4</sup>) and equivalent isotropic displacement parameters (Å<sup>2</sup> x 10<sup>3</sup>) for sad. U(eq) is defined as one third of the trace of the orthogonalized Uij tensor.

	x	y	z	U(eq)
Br(1)	9821(1)	2003(1)	6347(1)	57(1)
C(1)	8935(2)	2383(6)	6516(2)	41(1)
C(2)	8806(2)	3714(6)	6939(2)	45(1)
C(3)	8170(2)	4021(6)	7070(2)	43(1)
C(4)	7663(2)	2941(5)	6776(2)	35(1)
C(5)	6959(2)	2884(5)	6843(2)	36(1)
C(6)	6583(2)	3899(6)	7224(2)	41(1)
C(7)	5921(2)	3554(6)	7203(2)	47(1)

			Sad. tax	
C(8)	5619(2)	2228(6)	6809(2)	48(1)
C(9)	5993(2)	1197(6)	6421(2)	41(1)
C(10)	6561(2)	1522(5)	6465(2)	33(1)
C(11)	7180(2)	589(5)	6087(2)	33(1)
C(12)	7801(2)	1599(5)	6342(2)	35(1)
C(13)	8438(2)	1308(5)	6209(2)	39(1)
C(14)	7197(2)	-1543(5)	6181(2)	33(1)
C(15)	6684(2)	-2225(5)	5677(2)	32(1)
C(16)	6342(2)	-3881(5)	5637(2)	35(1)
C(17)	5875(2)	-4173(6)	5137(2)	40(1)
C(18)	5753(2)	-2834(6)	4689(2)	45(1)
C(19)	6102(2)	-1172(6)	4724(2)	41(1)
C(20)	6567(2)	-876(5)	5222(2)	33(1)
C(21)	7001(2)	779(5)	5376(2)	37(1)

Table 3. Bond lengths [Å] and angles [deg] for sad.

Br(1)-C(1)	1.901(4)
C(1)-C(2)	1.376(6)
C(1)-C(13)	1.390(6)
C(2)-C(3)	1.375(6)
C(3)-C(4)	1.393(5)
C(4)-C(12)	1.403(5)
C(4)-C(5)	1.458(6)
C(5)-C(6)	1.395(5)
C(5)-C(10)	1.406(5)
C(6)-C(7)	1.370(6)
C(7)-C(8)	1.385(6)
C(8)-C(9)	1.409(6)
C(9)-C(10)	1.376(6)
C(10)-C(11)	1.535(5)
C(11)-C(12)	1.514(5)
C(11)-C(14)	1.553(5)
C(11)-C(21)	1.558(5)
C(12)-C(13)	1.375(5)
C(14)-C(15)	1.514(5)
C(15)-C(16)	1.382(5)
C(16)-C(20)	1.391(5)
C(16)-C(17)	1.385(5)
C(17)-C(18)	1.377(6)
C(18)-C(19)	1.393(6)
C(19)-C(20)	1.379(5)
C(20)-C(21)	1.503(5)
C(2)-C(1)-C(13)	122.0(4)
C(2)-C(1)-Br(1)	118.9(3)
C(13)-C(1)-Br(1)	119.0(3)
C(1)-C(2)-C(3)	120.2(4)
C(2)-C(3)-C(4)	118.9(4)
C(3)-C(4)-C(12)	120.3(4)
C(3)-C(4)-C(5)	131.2(4)
C(12)-C(4)-C(5)	108.5(3)
C(6)-C(5)-C(10)	120.3(4)
C(6)-C(5)-C(4)	130.8(4)
C(10)-C(5)-C(4)	108.9(3)
C(7)-C(6)-C(5)	119.2(4)
C(6)-C(7)-C(8)	121.2(4)
C(7)-C(8)-C(9)	120.2(4)
C(10)-C(9)-C(8)	118.9(4)
C(9)-C(10)-C(5)	120.3(4)
C(9)-C(10)-C(11)	129.7(3)
C(5)-C(10)-C(11)	110.1(3)
C(12)-C(11)-C(10)	101.4(3)
C(12)-C(11)-C(14)	115.0(3)
C(10)-C(11)-C(14)	112.1(3)
C(12)-C(11)-C(21)	114.8(3)
C(10)-C(11)-C(21)	111.4(3)
C(14)-C(11)-C(21)	102.6(3)
C(13)-C(12)-C(4)	120.5(4)
C(13)-C(12)-C(11)	128.4(3)
C(4)-C(12)-C(11)	111.1(3)
C(12)-C(13)-C(1)	118.1(4)

	Sad.tex
C(15)-C(14)-C(11)	102.9(3)
C(16)-C(15)-C(20)	120.9(3)
C(16)-C(15)-C(14)	129.1(3)
C(20)-C(15)-C(14)	109.9(3)
C(15)-C(16)-C(17)	118.8(3)
C(16)-C(17)-C(18)	120.5(4)
C(17)-C(18)-C(19)	120.9(4)
C(20)-C(19)-C(18)	118.7(4)
C(19)-C(20)-C(15)	120.2(4)
C(19)-C(20)-C(21)	129.5(3)
C(15)-C(20)-C(21)	110.2(3)
C(20)-C(21)-C(11)	102.8(3)

Symmetry transformations used to generate equivalent atoms:

Table 4. Anisotropic displacement parameters ( $\text{\AA}^2 \times 10^3$ ) for sad.  
The anisotropic displacement factor exponent takes the form:  
 $-2 \pi^2 [h^2 a^{*2} U_{11} + \dots + 2 h k a^* b^* U_{12}]$

	U11	U22	U33	U23	U13	U12
Br(1)	43(1)	50(1)	78(1)	-5(1)	0(1)	-5(1)
C(1)	45(2)	36(2)	42(2)	6(2)	1(2)	-6(2)
C(2)	57(3)	36(2)	40(2)	-2(2)	-6(2)	-14(2)
C(3)	64(3)	31(2)	33(2)	-7(2)	2(2)	-7(2)
C(4)	54(2)	23(2)	26(2)	4(2)	-1(2)	-3(2)
C(5)	53(2)	25(2)	29(2)	7(2)	1(2)	0(2)
C(6)	61(3)	29(2)	32(2)	-2(2)	1(2)	7(2)
C(7)	62(3)	41(3)	39(2)	1(2)	12(2)	11(2)
C(8)	53(3)	42(3)	49(2)	5(2)	6(2)	3(2)
C(9)	52(3)	30(2)	39(2)	2(2)	5(2)	-4(2)
C(10)	49(2)	20(2)	30(2)	7(2)	1(2)	-1(2)
C(11)	42(2)	25(2)	30(2)	-1(2)	1(2)	-3(2)
C(12)	52(3)	23(2)	29(2)	2(2)	1(2)	-2(2)
C(13)	51(3)	28(2)	37(2)	0(2)	1(2)	-5(2)
C(14)	45(2)	23(2)	31(2)	0(2)	-2(2)	0(2)
C(15)	39(2)	26(2)	29(2)	-2(2)	2(2)	0(2)
C(16)	44(2)	26(2)	37(2)	1(2)	4(2)	0(2)
C(17)	45(2)	28(2)	47(2)	-5(2)	4(2)	-7(2)
C(18)	49(2)	44(3)	39(2)	-6(2)	-7(2)	-4(2)
C(19)	56(3)	37(2)	30(2)	3(2)	-2(2)	0(2)
C(20)	48(2)	25(2)	27(2)	-2(2)	5(2)	-1(2)
C(21)	50(2)	28(2)	31(2)	3(2)	3(2)	-5(2)

Table 5. Hydrogen coordinates ( $\times 10^4$ ) and isotropic displacement parameters ( $\text{\AA}^2 \times 10^3$ ) for sad.

	x	y	z	U(eq)
H(2A)	9158	4423	7141	54
H(3A)	8077	4954	7356	51
H(6A)	6785	4817	7494	49
H(7A)	5663	4236	7463	56
H(8A)	5158	2013	6800	58
H(9A)	5788	292	6148	49
H(13A)	8535	399	5917	47
H(14A)	7639	-2053	6129	40
H(14B)	7077	-1883	6595	40
H(16A)	6426	-4801	5948	43
H(17A)	5637	-5306	5103	48
H(18A)	5426	-3047	4352	54
H(19A)	6021	-260	4410	50
H(21A)	6760	1948	5271	44
H(21B)	7401	736	5155	44